# Measurements of wind turbulence parameters by a conically scanning coherent Doppler lidar in the atmospheric boundary layer

Igor N. Smalikho, Viktor A. Banakh

V.E. Zuev Institute of Atmospheric Optics SB RAS, Tomsk, Russia

*Correspondence to*: Igor N. Smalikho (smalikho@iao.ru)

**Abstract.** The method and results of lidar studies of spatiotemporal variability of wind turbulence in the atmospheric boundary layer are reported. The measurements were conducted by a Stream Line pulsed coherent Doppler lidar with the use of conical scanning by a probing beam around the vertical axis. Lidar data are used to estimate the kinetic energy of turbulence, turbulent energy dissipation rate, integral scale of turbulence, and momentum fluxes. The dissipation rate was determined from the azimuth structure function of radial velocity within the inertial subrange of turbulence. When estimating the kinetic energy of turbulence from lidar data, we took into account the averaging of radial velocity over the sensing volume. The integral scale of turbulence was determined on the assumption that the structure of random irregularities of the wind field is described by the von Karman model. The domain of applicability of the used method and the accuracy of estimation of turbulence parameters were determined. Turbulence parameters estimated from Stream Line lidar measurement data and from data of a sonic anemometer were compared.

## 1 Introduction

Pulsed coherent Doppler lidars (PCDLs) are applied in various fields of scientific research, in particular, to study dynamic processes in the atmosphere, aircraft wake vortices, and wind turbine wakes (Banakh and Smalikho, 2013). PCDLs are quite promising for obtaining reliable estimates of wind turbulence parameters from lidar measurements in the entire atmospheric boundary layer (Eberhard et al., 1989; Gal-Chen and Eberhard, 1992; Frehlich et al., 1998; Frehlich and Cornman, 2002; Davies et al., 2004; Smalikho et al., 2005; Banta et al., 2006; Frehlich et al., 2006; O'Connor et al., 2010; Banakh and Smalikho, 2013; Sathe and Mann, 2013; Smalikho and Banakh, 2013; Smalikho et al., 2013; Sathe et al., 2015). For this purpose, different measurement geometries were proposed, and methods were developed for estimation of turbulence parameters, in particular, with allowance made for averaging of the radial velocity over the sensing volume and for the instrumental measurement error. Here, the radial velocity $V_r$ is understood as a projection of the wind vector $\mathbf{V} = \{V_z, V_x, V_y\}$ ($V_z$ is the vertical component, $V_x$ and $V_y$ are the horizontal components) onto the axis of the probing beam at the point $\mathbf{r} = \{z, x, y\} = R\mathbf{S}$, where $R$ is the distance from the lidar, $\mathbf{S} = \{\sin\varphi, \cos\varphi\cos\theta, \cos\varphi\sin\theta\}$, $\varphi$ is the elevation angle, and $\theta$ is the azimuth angle. Denote the average wind velocity and the wind direction angle as $U$ and $\theta_V$, respectively, and fluctuations of the vertical, longitudinal, and transverse wind components as $w$, $u$, and $v$.

The use of the conical scanning by the probing beam (when the elevation angle $\varphi$ is fixed during measurements, while the azimuth angle $\theta = \omega_s t$ varies in time $t$ with the constant angular rate $\omega_s$) allows reconstruction of not only the wind speed and direction, but also vertical profiles of different wind turbulence parameters from measurements by PCDL. It was shown by Eberhard et al. (1989) that the kinetic energy of turbulence $E = (\sigma_w^2 + \sigma_u^2 + \sigma_v^2)/2$ can be determined from measurements by conically scanning PCDL at the elevation angle $\varphi$ = 35.3°, where $\sigma_w^2 = < w^2 >$, $\sigma_u^2 = < u^2 >$, $\sigma_v^2 = < v^2 >$, and the angular brackets denote the ensemble averaging. However, in the results for $E$, the effect of averaging of the radial velocity over the sensing volume (see Eq.(6) in paper of Smalikho and Banakh, 2013) was not taken into account. A method for reconstructing the vertical profiles of the fluxes of momentum $< uw >$ and $< vw >$ was also proposed by Eberhard et al. (1989).

Methods for determination of the turbulent energy dissipation rate $\varepsilon$ and the integral scale of turbulence $L_V = \int_0^\infty dr\, B_{||}(r)/\sigma_r^2$, where $B_{||}(r)$ is the longitudinal correlation function and $\sigma_r^2 = B_{||}(0)$ is the variance of the radial wind velocity, from measurements by conically scanning PCDL have been proposed (Frehlich et al., 2006; Smalikho and Banakh, 2013; Smalikho et al. 2013). In this case, turbulence parameters are estimated through fitting of the theoretically calculated azimuth (transverse) structure function of the radial velocity measured by the lidar to the corresponding measured function on the assumption that turbulence is isotropic and its spatial structure is described by the von Karman model (Vinnichenko et al., 1973). However, if the radius of the scanning cone base $R' = R\cos\varphi$, where $R$ is the distance between the lidar and the center of the sensing volume, is comparable with or smaller than $L_V$, then the method of the azimuth structure function can give a large error in estimates of wind turbulence parameters (Smalikho and Banakh, 2013).

Pulsed coherent Doppler lidars capable of providing measured data with high spatial resolution (longitudinal size of the sensing volume can be around 30 m), for example, Stream Line lidars (HALO Photonics) and Windcube lidars (Leosphere) are now widely used in practice. In this paper, for lidars of this type, we propose a method for determination of wind turbulence parameters from measurements by conically scanning PCDLs, which removes the mentioned disadvantages of the earlier methods. With the use of the proposed method, we have obtained the time and height distributions of $E$, $\varepsilon$, $L_V$, $< uw >$, and $< vw >$ in the atmospheric layer from 100 to 500 m in altitude from data of an atmospheric experiment with the Stream Line lidar. The accuracy of the obtained results is analyzed.

## 2 Basic equations

First, we describe the equations that will be used to develop the measurement strategy and the procedure of estimation of wind turbulence parameters: $E$, $\varepsilon$, and $L_V$. Instantaneous values of components of the wind velocity vector are random functions of coordinates and time, that is, $\mathbf{V} = \mathbf{V}(\mathbf{r}, t)$. The radial velocity at a point moving in the cone base of conical scanning as the azimuth angle $\theta$ changes from 0° to 360° (or in radians from 0 to $2\pi$) can be represented in the form

$$V_r(\theta) = \mathbf{S}(\theta) \cdot \mathbf{V}(R\mathbf{S}(\theta), \theta / \omega_s), \tag{1}$$

where $\varphi$, $R$, and $\omega_s$ are constant parameters.

The turbulence is assumed to be stationary (for time scales no shorter than 1 hour) and horizontally homogeneous (within the scanning cone base). Because of anisotropy of wind turbulence, the variance of the radial velocity $\sigma_r^2 = <[V_r'(\theta)]^2>$, where $V_r' = V_r - <V_r>$, is a function of the azimuth angle: $\sigma_r^2 = \sigma_r^2(\theta)$. For the variance of the radial velocity averaged over the azimuth angles

$$\bar{\sigma}_r^2 = (2\pi)^{-1} \int_0^{2\pi} d\theta \, \sigma_r^2(\theta), \tag{2}$$

from Eqs. (1) and (2) after the corresponding ensemble averaging and integration over the angle $\theta$, we obtain the equation

$$\bar{\sigma}_r^2 = (\sin\varphi)^2 \sigma_w^2 + (1/2)(\cos\varphi)^2 (\sigma_u^2 + \sigma_v^2). \tag{3}$$

From Eq. (3) at the angle $\varphi = \varphi_E = \tan^{-1}(1/\sqrt{2}) \approx 35.3°$, we can find a simple relation between the kinetic energy of turbulence $E$ and the variance $\bar{\sigma}_r^2$ in the form (Eberhard et al., 1989)

$$E = (3/2)\bar{\sigma}_r^2. \tag{4}$$

Consider the azimuth structure function of the radial velocity $D_r(\psi;\theta) = <[V_r'(\theta+\psi) - V_r'(\theta)]^2>$ ($\psi > 0$). For this function at $\psi \le \pi/2$ (90°) and the fast movement of a point in a circle of the radius $R' = R\cos\varphi$, when the condition $R'\omega_s >> |<\mathbf{V}>|$ is true, the transfer of turbulent inhomogeneities by the average flow can be neglected. Due to anisotropy of turbulence, the function $D_r(\psi;\theta)$, in the general case, depends on the angle $\theta$. By analogy with Eq. (2), we introduce the averaged structure function

$$\bar{D}_r(\psi) = (2\pi - \psi)^{-1} \int_0^{2\pi-\psi} d\theta \, D_r(\psi;\theta). \tag{5}$$

Under the condition $\psi R' << L_V$, due to the local isotropy of turbulence, $D_r(\psi;\theta)$ is independent of $\theta$, and $\bar{D}_r(\psi) = D_r(\psi)$. In addition, if the condition $R' > L_V$ is also fulfilled, then, according to the Kolmogorov theory, $D_r(\psi)$ is described by the equation (Kolmogorov, 1941)

$$D_r(\psi) = (4/3) C_K (\varepsilon \psi R')^{2/3}, \tag{6}$$

where $C_{\mathrm{K}} \approx 2$ is the Kolmogorov constant.

To find the relation between the structure function $\bar{D}_r(\psi)$ and the integral scale $L_V$, it is necessary to know the equation for the correlation tensor of wind turbulence $B_{\alpha\beta}(\mathbf{r}) = \langle V'_\alpha(\mathbf{r}_0+\mathbf{r})V'_\beta(\mathbf{r}_0)\rangle$ ($\alpha, \beta = z, x, y$; $V' = V - \langle V \rangle$), which can be readily found for the case of isotropic turbulence using an appropriate model for $B_{\parallel}(r)$. To find this relation, we assume that turbulence is isotropic, and within this assumption $\bar{D}_r(\psi) = D_r(\psi)$. Upon generalization of Eq. (19) given in (Smalikho and Banakh, 2013) for $\varphi$ = 0°, for the case of an arbitrary elevation angle, we have derived the following equation

$$D_r(\psi) = 4\int_0^\infty d\kappa S_{\parallel}(\kappa)[1-\mu_1\cos(2\pi r'\kappa)+\mu_2\pi r'\kappa\sin(2\pi r'\kappa)], \tag{7}$$

where $\mu_1 = (\cos\varphi)^2\cos\psi + (\sin\varphi)^2$,

$\mu_2 = (\cos\varphi)^2(1+\cos\psi)/2 + (\sin\varphi)^2$,

$r' = R'\sqrt{2(1-\cos\psi)}$,

and $S_{\parallel}(\kappa) = 2\int_0^\infty dr\, B_{\parallel}(r)\cos(2\pi\kappa r)$ is the longitudinal spatial spectrum of wind velocity fluctuations. If the condition $R' = R\cos\varphi >> L_V$ is fulfilled, in Eq. (7) we can set $\mu_1 = \mu_2$ = 1, $r' = y' = \psi R'$ (here, the angle $\psi$ is in radians), and then for any angles $\psi \le 180°$ the azimuth structure function $D_r(\psi)$ coincides with the transverse structure function

$$D_{\perp}(y') = 4\int_0^\infty d\kappa\, S_{\perp}(\kappa)[1-\cos(2\pi y'\kappa)], \tag{8}$$

where $S_{\perp}(\kappa) = [S_{\parallel}(\kappa) - \kappa dS_{\parallel}(\kappa)/d\kappa]/2$ is the transverse spectrum of wind velocity fluctuations (Lumley and Panofsky, 1964; Monin and Yaglom, 1971).

For the spectrum $S_{\parallel}(\kappa)$, we use the von Karman model (Vinnichenko et al., 1973; Smalikho and Banakh, 2013):

$$S_{\parallel}(\kappa) = 2\sigma_r^2 L_V[1+(C_1 L_V\kappa)^2]^{-5/6}, \tag{9}$$

where $C_1$ = 8.4134. For this model, the following relationship is true

$$\sigma_r^2 = C_2(\varepsilon L_V)^{2/3}. \tag{10}$$

In Eq. (10) at $C_{\mathrm{K}}$ = 2, the coefficient $C_2$ = 1.2717 (Smalikho and Banakh, 2013).

Figure 1 shows the results of calculation of the normalized structure functions $D_r(\psi)/\sigma_r^2$ and $D_{\perp}(R'\psi)/\sigma_r^2$ at $\varphi = \varphi_E \approx 35.26°$ and different values of the ratio $R'/L_V$. It can be seen that the higher the ratio, the smaller the difference between the functions. Calculations at $R'/L_V \ge 4$ demonstrate the nearly complete coincidence of the structure functions described by Eqs. (7) and (8) for any angles $\psi \le 180°$. The nearly complete coincidence is also observed at $\psi \le 9°$ for any $R'/L_V \ge 1/4$. At the same time, if the condition $R'/L_V << \psi^{-1}$ is fulfilled, then, with allowance for Eq. (10), both structure functions $D_r(\psi)$ and $D_\perp(R'\psi)$ are described by Eq. (6).

We introduce the parameter $\gamma$ characterizing the degree of deviation of $D_\perp(R'\psi)$ from $D_r(\psi)$ as

$$\gamma = \{L^{-1}\sum_{l=1}^{L}[D_r(l\Delta\theta)/D_\perp(R'l\Delta\theta)-1]^2\}^{1/2}, \quad (11)$$

where $\Delta\theta$ = 3° and $L$ = 30. Using the data of Fig. 1, we have calculated the parameter $\gamma$ by this equation and obtained the following results: $\gamma$ = 0.21 at $R'/L_V$ = 0.5; $\gamma$ = 0.08 at $R'/L_V$ = 1, and $\gamma$ = 0.02 at $R'/L_V$ = 2. It should be noted that if we fit the function $D_\perp(R'l\Delta\theta)$ with arbitrary values of $\varepsilon$ and $L_V$ by the least-square method (see Eqs. (13)–(16) in paper of Smalikho and Banakh (2013)) to the function $D_r(l\Delta\theta)$ obtained at $R'/L_V$ = 0.5, then we can attain a significant decrease in the parameter $\gamma$ (six times in comparison with the above values), but the estimates of $L_V$ and $\sigma_r^2$ exceed the true values of these parameters more than twice, although the error of $\varepsilon$ estimation by this method is about 15%. Therefore, for these situations (when the ratio $R'/L_V$ < 1), it is possible to obtain the more accurate result through direct determination of the variance $\sigma_r^2$ and the dissipation rate $\varepsilon$ (the dissipation rate is determined from the azimuth structure function of the radial velocity within the inertial subrange of turbulence with the use of Eq. (6)) and then calculation of the integral scale $L_V$ by Eq. (10).

## 3 Measurement strategy and estimation of turbulence parameters

To obtain the information about the kinetic energy, its dissipation rate, and the integral scale of turbulence from the same raw lidar data, it is proposed, according to the previous section, to use the conical scanning by the probing beam at the elevation angle $\varphi = \varphi_E \approx 35.3°$ in the experiment. During the measurements, the azimuth angle changes starting from 0° with the constant angular rate $\omega_s = 2\pi / T_{\text{scan}}$, where $T_{\text{scan}}$ is the time of one scan. As an angle of 360° is achieved, the scanning in the opposite direction starts practically immediately. This cycle is repeated many times during the experiment.

An array of estimates of the radial velocity $V_{\text{L}}(\theta_m, R_k, n)$ is obtained from signals recorded by the PCDL receiving system after the corresponding pre-processing (Banakh et al., 2016). Here, $\theta_m = m\Delta\theta$ is the azimuth angle; $m = 0, 1, 2, ..., M-1$; $\Delta\theta$ is the azimuth resolution; $R_k = R_0 + k\Delta R$ is the distance from the lidar to the center of the sensing volume; $R_0$ is the distance to the first usable range gate; $k = 0, 1, 2, ..., K$; $\Delta R$ is a range gate length, and $n = 1, 2, 3, ..., N$ is the number of full conical scans. Uncertainty in the radial velocity measurement depends on the signal-to-noise ratio (SNR). At low SNR the probability of "bad" estimate of the radial velocity randomly taking any values in the chosen receiver band (for example,

$\pm 19,4$ m/s for the Stream Line lidar), regardless of the true value of the velocity, can significantly differ from zero. To avoid the application of the data filtering procedure, the measured array $V_{\mathrm{L}}(\theta_m, R_k, n)$ must not contain “bad” estimates. Then, the lidar estimate of the radial velocity can be represented as (Frehlich and Cornman, 2002; Banakh and Smalikho, 2013)

$$V_{\mathrm{L}}(\theta_m, R_k, n) = V_a(\theta_m, R_k, n) + V_e(\theta_m, R_k, n)\,, \qquad (12)$$

where $V_a(\theta_m)$ is the radial velocity averaged over the sensing volume with the longitudinal dimension $\Delta z$ and the transverse dimension $\Delta y_k = \Delta\theta R_k \cos\varphi_E$ (here, $\Delta\theta$ is in radians), and $V_e(\theta_m)$ is the random instrumental error of estimation of the radial velocity having the following properties: $< V_e > = < V_a V_e > = 0$ and $< V_e(\theta_m) V_e(\theta_l) > = \sigma_e^2 \delta_{m-l}$ ($\sigma_e^2$ is the variance of random error, $\delta_m$ is the Kronecker delta). For the conditions of stationary and homogeneous turbulence, the estimate is unbiased, that is, $< V_{\mathrm{L}}(\theta_m, R_k, n) > = < V_r(\theta_m, R_k) >$.

Lidars of Stream Line type, one of which is used in our experiments, are characterized by formation of a sensing volume of relatively small size, for example, with the longitudinal dimension $\Delta z$ = 30 m (Pearson et al., 2009). When the conical scanning with $\varphi = \varphi_E$ and $\Delta\theta$ = 3° is used, the transverse dimension of the sensing volume increases linearly from 8.5 m at $R_k$ = 200 m to 42.8 m at $R_k$ = 1 km. It is important to take into account the effect from averaging of the radial velocity over the sensing volume not only when estimating the dissipation rate $\varepsilon$ within the inertial subrange of turbulence, but also when estimating the parameters $E$ and $L_V$, especially, when $L_V$ exceeds the size of the sensing volume insignificantly. Even at the high signal-to-noise ratio and the large number of probing pulses used for accumulation of lidar data, when the variance $\sigma_e^2$ is extremely small, it is necessary to take into account the instrumental error of estimation of the radial velocity, if turbulence is very weak (Frehlich et al., 2006).

After the corresponding manipulations, from Eq. (12), taking into account statistical properties of the random error $V_e(\theta_m)$, we derived the following equations for the variance and the structure function of lidar estimate of the radial velocity averaged over all azimuth angles $\theta_m$:

$$\bar{\sigma}_{\mathrm{L}}^2 = \bar{\sigma}_a^2 + \sigma_e^2\,, \qquad (13)$$

$$\bar{D}_{\mathrm{L}}(\psi_l) = \bar{D}_a(\psi_l) + 2\sigma_e^2\,, \qquad (14)$$

where $\bar{\sigma}_\alpha^2 = M^{-1} \sum_{m=0}^{M-1} \sigma_\alpha^2(\theta_m)$ ; $\sigma_\alpha^2(\theta_m) = < [V'_\alpha(\theta_m)]^2 >$ ; $\bar{D}_\alpha(\psi_l) = (M-l)^{-1} \sum_{m=0}^{M-1-l} D_\alpha(\psi_l, \theta_m)$ ; $D_\alpha(\psi_l, \theta_m)$ = $< [V'_\alpha(\theta_m + \psi_l) - V'_\alpha(\theta_m)]^2 >$; $V'_\alpha = V_\alpha - < V_r >$ and subscript $\alpha$ is L or $a$. In Eqs. (13) and (14) it is assumed that $\sigma_e$ is independent of the azimuth angle $\theta_m$. The variance $\bar{\sigma}_a^2$ can be represented as

$$\bar{\sigma}_a^2 = \bar{\sigma}_r^2 - \bar{\sigma}_t^2 , \tag{15}$$

where $\bar{\sigma}_t^2 = M^{-1}\sum_{m=0}^{M-1}\sigma_t^2(\theta_m)$ and $\sigma_t^2(\theta_m) = \sigma_r^2(\theta_m) - \sigma_a^2(\theta_m)$ is turbulent broadening of the Doppler spectrum (Banakh and Smalikho, 2013).

Having specified the high resolution in the azimuth angle (large number $M$ ) and $\varphi = \varphi_E$ , from Eqs. (13) - (15) with allowance made for Eq. (4), we obtain the equation for the kinetic energy of turbulence in the form

$$E = (3/2)[\bar{\sigma}_{\mathrm{L}}^2 - \bar{D}_{\mathrm{L}}(\psi_1)/2 + G] , \tag{16}$$

where $G = \bar{\sigma}_t^2 + \bar{D}_a(\psi_1)/2$. At $L_V > \max\{\Delta z, \Delta y_k\}$, the dimensions of the sensing volume do not exceed the low-frequency boundary of the inertial subrange, for which turbulence is locally isotropic and, correspondingly, $G \sim \varepsilon^{2/3}$. If the condition $l\Delta y_k << L_V$ is additionally fulfilled, then for calculation of the turbulent broadening of the Doppler spectrum $\bar{\sigma}_t^2 = \sigma_t^2$ and the structure function $\bar{D}_a(\psi_l) = D_a(\psi_l)$ we can use the two-dimensional spatial Kolmogorov—Obukhov spectrum. For these conditions, the Gaussian temporal profile of the probing pulse, and the rectangular time window used for obtaining of Doppler spectra, we have derived the following equations (Banakh and Smalikho, 2013):

$$\sigma_t^2 = \varepsilon^{2/3} F(\Delta y_k) , \tag{17}$$

$$D_a(\psi_l) = \varepsilon^{2/3} A(l\Delta y_k) . \tag{18}$$

In Eqs. (17) and (18)

$$F(\Delta y_k) = \int_0^\infty d\kappa_1 \int_0^\infty d\kappa_2 \Phi(\kappa_1,\kappa_2)[1 - H_{\|}(\kappa_1)H_{\perp}(\kappa_2)] , \tag{19}$$

$$A(l\Delta y_k) = 2\int_0^\infty d\kappa_1 \int_0^\infty d\kappa_2 \Phi(\kappa_1,\kappa_2) H_{\|}(\kappa_1)H_{\perp}(\kappa_2)[1 - \cos(2\pi l \Delta y_k \kappa_2)] , \tag{20}$$

where $\Phi(\kappa_1,\kappa_2) = C_3(\kappa_1^2+\kappa_2^2)^{-4/3}[1+(8/3)\kappa_2^2/(\kappa_1^2+\kappa_2^2)]$ ; $C_3 = 2C_2/(3\pi C_1^{2/3})$ = 0.0652; $H_{\|}(\kappa_1) = [\exp\{-(\pi\Delta p\kappa_1)^2\}\mathrm{sinc}(\pi\Delta R\kappa_1)]^2$ is the longitudinal transfer function of the low-frequency filter, and $H_{\perp}(\kappa_2) = [\mathrm{sinc}(\pi\Delta y_k \kappa_2)]^2$ is the transverse one; $\Delta p = c\sigma_p/2$; $c$ is the speed of light; $2\sigma_p$ is the duration of the probing pulse determined by the $e^{-1}$ power level to right and to the left from the peak point, $\Delta R = cT_W/2$, $T_W$ is the temporal window width; and $\mathrm{sinc}(x) = \sin x / x$.

In Eq. (16), $\bar{\sigma}_{\mathrm{L}}^2$ and $\bar{D}_{\mathrm{L}}(\psi_1)$ are directly determined from experimental data. To take into account the term $G = \varepsilon^{2/3}[F(\Delta y_k) + A(\Delta y_k)/2]$ in Eq. (16), it is necessary to have information about the dissipation rate $\varepsilon$. According to

Eq. (14), the difference $\bar{D}_{\mathrm{L}}(\psi_l)-\bar{D}_{\mathrm{L}}(\psi_1)$ is equal to the difference $\bar{D}_a(\psi_l)-\bar{D}_a(\psi_1)$. Within the framework of the above conditions and according to Eq. (18), the latter is equal to $\varepsilon^{2/3}[A(l\Delta y_k)-A(\Delta y_k)]$. Then the dissipation rate can be determined as

$$\varepsilon=\left[\frac{\bar{D}_{\mathrm{L}}(\psi_l)-\bar{D}_{\mathrm{L}}(\psi_1)}{A(l\Delta y_k)-A(\Delta y_k)}\right]^{3/2}, \tag{21}$$

where the number $l>1$ should be so that, on the one hand, the consideration is within the inertial subrange and, on the other hand, the condition

$$[\bar{D}_{\mathrm{L}}(\psi_l)-\bar{D}_{\mathrm{L}}(\psi_1)]>>\bar{D}_{\mathrm{L}}(\psi_1)\sqrt{2/(MN)} \tag{22}$$

is fulfilled. This condition provides for the high accuracy of estimation of the dissipation rate at the large numbers $M$ and $N$. In parallel, we can calculate the instrumental error of estimation of the radial velocity $\sigma_e$ as

$$\sigma_e=\sqrt{[\bar{D}_{\mathrm{L}}(\psi_1)-\varepsilon^{2/3}A(\Delta y_k)]/2}\equiv\sqrt{\frac{\bar{D}_{\mathrm{L}}(\psi_1)A(l\Delta y_k)-\bar{D}_{\mathrm{L}}(\psi_l)A(\Delta y_k)}{2[A(l\Delta y_k)-A(\Delta y_k)]}}. \tag{23}$$

Using the lidar estimates of the kinetic energy $E$ (by Eq. (16)) and the dissipation rate $\varepsilon$ from experimental data, we can determine the integral scale $L_V$ by Eqs. (4) and (10) as

$$L_V=C_4E^{3/2}/\varepsilon, \tag{24}$$

where $C_4=[2/(3C_2)]^{3/2}$ = 0.3796.

Taking into account that the elevation angle $\varphi=\varphi_E=\tan^{-1}\left(1/\sqrt{2}\right)$, we use the following equation (Eberhard et al., 1989) for determination of the momentum fluxes $<uw>$ and $<vw>$:

$$<uw>+j<vw>=\frac{3}{\sqrt{2}}\frac{1}{M}\sum_{m=0}^{M-1}\sigma_{\mathrm{L}}^2(\theta_m)\exp[j(\theta_m-\theta_V)], \tag{25}$$

where $j=\sqrt{-1}$. Since the instrumental error of estimation of the radial velocity $\sigma_e$ is independent of the azimuth angle $\theta_m$ and within the sensing volume, turbulence is locally isotropic (the condition $L_V>\max\{\Delta z,\Delta y_k\}$ is assumed to be true), that is $\sigma_t^2$ does not depend on $\theta_m$, it is not necessary here to take into account the instrumental error and the effect from averaging of the radial velocity over the sensing volume. Indeed, as shown by Eberhard et al. (1989), in the case of a horizontally homogeneous turbulence statistics and very large $M$, equation (25) is exact, if $\sigma_{\mathrm{L}}^2(\theta_m)$ is replaced by $\sigma_r^2(\theta_m)$.

On the other hand, $\sigma_{\mathrm{L}}^2(\theta_m) = \sigma_r^2(\theta_m) - \sigma_t^2 + \sigma_e^2$. Taking into account that $\sigma_t^2$ and $\sigma_e^2$ do not depend on $\theta_m$ and $\frac{1}{M}\sum_{m=0}^{M-1}\exp[j(\theta_m - \theta_V)] = 0$, Eq. (25) can also be regarded as exact.

With increasing range $R_k = R_0 + k\Delta R$, the measurement height $h_k = R_k \sin\varphi$ and the transverse dimension of the sensing volume $\Delta y_k = \Delta\theta R_k \cos\varphi$ increase linearly. Using Eqs. (19) and (20), we calculated $F(\Delta y_k)$ and $A(l\Delta y_k)$ by specifying the parameters of the lidar experiment conducted in 2016 (see Section 5), that is, $\varphi = \varphi_E$ = 35.3°, $\Delta\theta = \pi/60$ (3°), $\Delta R$ = 18 m and $\Delta p$ = 15.3 m. Without taking into account the spatial averaging of the radial velocity over the sensing volume, in Eq. (20) we set $H_{\|}(\kappa_1) = H_{\perp}(\kappa_2) = 1$ and $A(l\Delta y_k) = A_0(l\Delta y_k)$. Then, after integrating over $\kappa_1$ and $\kappa_2$ in Eq. (20), we obtain the following equation: $A_0(l\Delta y_k) = 2.667(l\Delta y_k)^{2/3}$ = $(4/3)C_{\mathrm{K}}(l\Delta y_k)^{2/3}$. According to Fig. 1, the azimuth and transverse structure functions of the radial velocity completely coincide under the condition $l\Delta\theta \leq$ 9°. Therefore, we carried out calculations of $A(l\Delta y_k)$ at $l$ = 1 and $l$ = 3. To estimate the turbulent energy dissipation rate by equation (21), we set $l$ = 3. Denote by $\varepsilon_0$ the dissipation rate estimate obtained after the replacement of the difference $A(3\Delta y_k) - A(\Delta y_k)$ by $A_0(3\Delta y_k) - A_0(\Delta y_k)$ in Eq. (21). The ratio $\varepsilon/\varepsilon_0 = \left\{[A_0(3\Delta y_k) - A_0(\Delta y_k)]/[A(3\Delta y_k) - A(\Delta y_k)]\right\}^{3/2}$ shows the degree of difference in the dissipation rate estimates with and without taking into account the averaging of the radial velocity over the sensing volume.

Figure 2 shows vertical profiles of $\Delta y_k$, $3\Delta y_k$, $F(\Delta y_k)$, $A(\Delta y_k)$, $A_0(\Delta y_k)$ $A(3\Delta y_k)$, $A_0(3\Delta y_k)$, $A(3\Delta y_k) - A(\Delta y_k)$, $A_0(3\Delta y_k) - A_0(\Delta y_k)$ and $\varepsilon/\varepsilon_0$. The dashed line corresponds to the value of the longitudinal dimension of the sensing volume calculated as $\Delta z = \Delta R/\mathrm{erf}\left(\Delta R/(2\Delta p)\right)$, where $\mathrm{erf}(x)$ is the error function (Banakh and Smalikho, 2013). It is seen that with increasing height $h_k$ the transverse dimension of the sensing volume increases and at heights greater than 400 m it becomes larger than the longitudinal dimension $\Delta z$, which does not depend on the measurement height. The $F(\Delta y_k)$ takes values of 5.8 m$^{2/3}$ at a height of 100 m and 8.3 m$^{2/3}$ at a height of 500 m (see Fig. 2 (b)). Fig. 2 (b) also illustrates the effect of spatial averaging of the radial velocity on the azimuth (transverse) structure function of the radial velocity within the inertial subrange of turbulence (if the condition $3\Delta y_k << L_V$ is satisfied). According to Fig. 2 (b), the ratio $A_0(\Delta y_k)/A(\Delta y_k)$ varies from 2.3 (at a height of 500 m) to 4.2 (at a height of 100 m) and the ratio $A_0(3\Delta y_k)/A(3\Delta y_k)$ varies from 1.4 (at a height of 500 m) to 2 (at a height of 100 m). As can be seen in Fig. 2 (c), the difference between $A(3\Delta y_k) - A(\Delta y_k)$ and $A_0(3\Delta y_k) - A_0(\Delta y_k)$ is much smaller and, according to Fig. 2 (d), the estimate of the dissipation rate without taking into account the averaging of the radial velocity over the sensing volume is understated by 1.5 times for a height of 100 m, and for heights above 375 m, the underestimation does not exceed 5%.

The practical implementation of the described method of estimation of the wind turbulence parameters $\varepsilon$, $E$, $L_V$, $<uw>$, and $<vw>$ consists in the following. The obtained array $V_{\mathrm{L}}(\theta_m, R_k, n)$ for every height $h_k = R_k \sin\varphi_E$ was used to determine the average wind vector $<\mathbf{V}>$ (average wind velocity $U$ and wind direction angle $\theta_V$) with the use of the least-square sine-wave fitting and the data of all $N$ scans. Then fluctuations of the radial velocity are calculated as $V_{\mathrm{L}}'(\theta_m, R_k, n) = V_{\mathrm{L}}(\theta_m, R_k, n) - \mathbf{S}(\theta_m) \cdot <\mathbf{V}>$, where $\mathbf{S}(\theta_m) = \{\sin\varphi_E, \cos\varphi_E \cos\theta_m, \cos\varphi_E \sin\theta_m\}$ (in place of the array $\mathbf{S}(\theta_m) \cdot <\mathbf{V}>$, it is also possible to use directly the calculated values of $V_{\mathrm{L}}'(\theta_m, R_k, n) = V_{\mathrm{L}}(\theta_m, R_k, n) - <V_{\mathrm{L}}(\theta_m, R_k, n)>$ at the nonideal horizontal homogeneity of the average wind). Here and in Eqs. (13)-(14), (16), (21)-(23), and (25), the ensemble averaging $<X>$ should be replaced with the averaging over scans $N^{-1}\sum_{n=1}^{N} X_n$. The number of scans $N$ necessary for the averaging of data was determined experimentally (see Section 5).

To test the described method for measurement of the wind turbulence parameters, we have conducted experiments with the conically scanning Stream Line lidar (the main parameters of the lidar can be found in Table 1 of paper of Banakh and Smalikho (2016)) and the sonic anemometer at a height of 43 m in 2014 and 2016.

## 4 Experiment of 2014

To study the feasibility of estimating the turbulence energy dissipation rate from PCDL data by the method described in Section 3 under various atmospheric conditions, we have conducted the five-day experiment in August 15-19 of 2014 at the Basic Experimental Complex (BEC) of Institute of Atmospheric Optics SB RAS. Experimental instrumentation included the Stream Line PCDL set at the central part of BEC mostly surrounded by forest and a sonic anemometer installed at the top of a tower (near BEC) at a height of 43 m from the ground. The separation between the lidar and the tower was 142 m (see Fig.3).

Conical scanning by the probing beam with an angular rate of 5°/s (duration of one scan $T_{\mathrm{scan}}$ = 72 s) at the elevation angle $\varphi$ = 9° was applied permanently during the experiment. For accumulation, $N_a$ = 3000 of probing pulses were used. Since the pulse repetition frequency of the Stream Line lidar is $f_p$ = 15 kHz, the measurement for every azimuth scanning angle took $N_a / f_p$ = 0.2 s. In this case, for one scan we have $M = T_{\mathrm{scan}} / (N_a / f_p)$ = 360 of such measurements with the resolution in the azimuth angle $\Delta\theta$ = 1°. Since the lidar telescope is at a height of 1 m above the surface and the elevation angle is 9°, the probing pulse reaches the height of the sonic anemometer (43 m) at a distance of 270 m. To increase the lidar signal-to-noise ratio in the height of 43 m, the focus of the lidar beam was set to 300 m. In Fig. 3, the blue circle shows the trajectory of the center of the sensing volume at a height of 43 m during the measurements.

From the array of radial velocities measured by the lidar in four full cycles of conical scanning ($N$ = 4) for approximately 5 min (for this time at $R$ = 270 m and $\varphi$ = 9°, the sensing volume passes the distance $8\pi R \cos\varphi$ equal to about 6.7 km), we have calculated the values of the azimuth structure function $\bar{D}_{\mathrm{L}}(\psi_1)$ and $\bar{D}_{\mathrm{L}}(\psi_l)$. We obtained lidar estimates of the turbulent energy dissipation rate $\varepsilon_{\mathrm{L}}$ by Eq. (21) ($\varepsilon$ should be replaced with $\varepsilon_{\mathrm{L}}$). To calculate the longitudinal structure functions $D_{\parallel}(r_1)$ and $D_{\parallel}(r_2)$ at separations of observation points $r_1 = \Delta t_1 U$ and $r_2 = \Delta t_2 U$ ($r_1, r_2 > 0$, $r_2 > r_1$; $\Delta t_1$ and $\Delta t_2$

are time separations), we used the array of longitudinal components of the wind vector measured by the sonic anemometer for the time $T$ = 20 min (at a sampling frequency of 10 Hz). For this time, at the average wind velocity $U$ = 5 m/s typical of the surface layer, air masses move to a distance $UT$ = 6 km, which is quite comparable with the corresponding value for the lidar data (about 6.7 km). We obtained estimates of the dissipation rate from the sonic anemometer data $\varepsilon_{\mathrm{S}}$ by the equation

$$\varepsilon_{\mathrm{S}} = \left[ \frac{D_{\|}(r_2) - D_{\|}(r_1)}{C_{\mathrm{K}} \cdot (r_2^{2/3} - r_1^{2/3})} \right]^{3/2}, \tag{26}$$

on the assumption that $l_V << r_1 < r_2 \le r_H$, where $l_V$ is the inner scale of turbulence and $r_H$ is the scale of the low-frequency boundary of the inertial subrange. Thus, the sample sizes for the lidar data and the sonic anemometer data are close, and the comparison of estimates of the dissipation rate $\varepsilon_{\mathrm{S}}$ and $\varepsilon_{\mathrm{L}}$ at properly specified $l$, $r_1$, $r_2$ and temporal synchronization of the results is quite justified.

According to the experimental data given in (Byzova et al., 1989), the upper boundary of the inertial subrange $r_H$ at a height of 43 m takes values no smaller than 20 m, at least, at the neutral, unstable, and weak stable temperature stratification of the atmospheric boundary layer. In our case, $\Delta y_k$ = 4.84 m, and for $l$ = 4 the condition $l\Delta y \le 20$ m is true. In processing of the sonic anemometer data, we specified $r_1$ = 5 m and $r_2$ = 20 m.

Lidar measurements were started at 18:00 LT on 8/15/2014 and finished at 14:30 LT on 8/19/2014. Unfortunately, because of the weather conditions (low SNR ) and some technical troubles, a part (around 15%) of lidar data appeared to be unusable for the processing. Nevertheless, we succeeded in obtaining results under different atmospheric conditions for five days.

All the results of estimation of the turbulent energy dissipation rate from the data measured by the sonic anemometer and the Stream Line lidar are shown in Fig. 4. One can see, in general, a rather good agreement between the results obtained from measurements by these devices. For calculation of the relative errors of estimation of the dissipation rate $E_{\mathrm{S}} = \sqrt{<(\varepsilon_{\mathrm{S}}/<\varepsilon_{\mathrm{S}}>-1)^2>} \times 100\%$ and $E_{\mathrm{L}} = \sqrt{<(\varepsilon_{\mathrm{L}}/<\varepsilon_{\mathrm{L}}>-1)^2>} \times 100\%$, we used the data of Fig. 4 obtained from measurements under relatively steady conditions from 12 to 18 LT on August 18. The errors appeared to be rather close: $E_{\mathrm{S}}$ = 19% and $E_{\mathrm{L}}$ = 20%.

Using the data of Fig. 4, we have compared all estimates of the turbulent energy dissipation rate obtained from joint (simultaneous) measurements by the lidar and the sonic anemometer. The result of comparison is shown in Fig. 5. Calculations of parameters characterizing discrepancies in the estimates of the dissipation rate $b_{\mathrm{LS}} = <(\varepsilon_{\mathrm{L}} - \varepsilon_{\mathrm{S}})/[(\varepsilon_{\mathrm{L}} + \varepsilon_{\mathrm{S}})/2]> \times 100\%$ and $\Delta_{\mathrm{LS}} = \sqrt{<(\varepsilon_{\mathrm{L}} - \varepsilon_{\mathrm{S}})^2/[(\varepsilon_{\mathrm{L}} + \varepsilon_{\mathrm{S}})^2/4]>} \times 100\%$ with the use of all points in Fig. 5 have shown that $b_{\mathrm{LS}}$ = - 10% and $\Delta_{\mathrm{LS}}$ = 45%. Thus, the lidar estimate $\varepsilon_{\mathrm{L}}$ is, on average, 10% smaller than the estimate of the dissipation rate from the data of sonic anemometer. If we assume that random errors of estimates from data of these devices are statistically independent and the variances of random errors are identical, the root-mean-square error of estimate of the dissipation rate is about 30%, which is 1.5 times higher than the value of $E_{\mathrm{L}}$ given above.

It can be easily seen from Fig. 5 that at $\varepsilon < 10^{-3}$ m$^2$/s$^3$, the lidar estimates of the dissipation rate $\varepsilon_{\mathrm{L}}$ are, on average, understated in comparison with the estimates $\varepsilon_{\mathrm{S}}$. According to Fig.4, the estimates of the dissipation rate taking values smaller than $10^{-3}$ m$^2$/s$^3$ were mostly obtained from nighttime measurements. As a rule, the temperature stratification is stable in nighttime, and then the upper boundary of the inertial subrange $r_H$ can be smaller than the spread in observation points $4\Delta y_k, r_2 \sim 20$ m taken in Eqs. (21) and (26). In this case, estimates of the dissipation rate from the lidar and sonic anemometer data are understated, but the lidar estimate is understated to a greater extent because of the averaging of radial velocity over the sensing volume. Using the points of Fig. 5, whose coordinates satisfy the conditions $\varepsilon_{\mathrm{S}} \geq 10^{-3}$ m$^2$/s$^3$ and $\varepsilon_{\mathrm{L}} \geq 10^{-3}$ m$^2$/s$^3$, we have obtained $b_{\mathrm{LS}}$ = 0 and $\Delta_{\mathrm{LS}}$ = 30%. On the assumption of independent estimates from the data of lidar and sonic anemometer and of the equal variances of estimates, the error of lidar estimate of the dissipation rate, which can be calculated as $E_{\mathrm{L}} = \Delta_{\mathrm{LS}} / \sqrt{2}$, is equal to 21%. Thus, for the conditions of moderate and strong turbulence, when $\varepsilon \geq 10^{-3}$ m$^2$/s$^3$, the lidar estimate of the turbulence energy dissipation rate is unbiased, while the relative standard error of the estimation is about 20%.

## 5 Experiment of 2016

To test of method for determining the kinetic energy, its dissipation rate, the integral scale of turbulence, and momentum fluxes as described in Section 3, we have carried out the five-day experiment from 19:00 (from here on, the local time is used everywhere) of July 20 to 15:00 of July 24, 2016, at BEC. The Stream Line lidar was set exactly at the same place as in Experiment of 2014 (see Fig. 3). The weather was clear during these days. The presence of forest fires in the Tomsk region provided lidar measurements with rather high signal-to-noise ratios.

The Stream Line lidar operated continuously during the experiment. The focus of the lidar beam was set to 500 m. The conical scanning with an angular rate of 6°/s (time of one full scan $T_{\mathrm{scan}}$ = 1 min) at the elevation angle $\varphi = \varphi_E$ = 35.3° was used. The number of probing pulses for data accumulation was $N_a$ = 7500, which corresponded to the duration of measurement for every azimuth scanning angle $T_a$ = 0.5 s. In this case, for one full scan we have $M = T_{\mathrm{scan}} / T_a$ = 120 such measurements with the resolution in the azimuth angle $\Delta\theta$ = 3°. The range gate length $\Delta R$ was taken equal to 18m (vertical resolution $\Delta h = \Delta R \sin\varphi_E \approx 10$ m).

In the processing of data of these measurements, we set the minimum useful range $R_0$ = 171 m, which corresponded to a minimum height of approximately 100 m. Except for the period from 5:00 to 9:00 LT of 7/21/2016, the probability of "bad" lidar estimates of the radial velocity was zero for the ranges from $R_0$ to almost 900 m. The maximum range $R_K$ was taken equal to 873 m, which corresponded to a height of about 500 m. In this experiment, the linear velocity of horizontal motion of the sensing volume (along the base of the scanning cone) $V_k = 2\pi \cos\varphi_E R_k / T_{\text{scan}}$ was 14.6 m/s for $R_k = R_0$ and 74.6 m/s for $R_k = R_K$. In this case, for one minute the center of the sensing volume passed a distance of, respectively, 876 m and 4476 m. In Fig. 3, red circles 1 and 2 show the trajectories of the lidar sensing volume at heights of, respectively, 100 and 500 m.

To obtain estimates of the wind turbulence parameters, raw data measured by some or other device for the time of 10 and 60 minutes are usually used. In our case, $T_{\text{scan}}$ = 1 min. This corresponds to the use of lidar data obtained for the number of full conical scans $N$ from 10 to 60. To determine the optimal number $N$, we selected the lidar data measured at night and day on July 22 of 2016 at a height of 200 m (1) from 01:00 to 07:00 and (2) from 12:00 to 18:00 LT. In these six-hour intervals, the horizontal wind speed averaged for 30 min varied from 11.5 to 13 m/s (night) and from 8 to 9.5 m/s (day).

Table 1 presents the averaged (for six-hour period) lidar estimates of the kinetic energy $E$ and the integral scale of turbulence $L_V$ obtained from measurements in daytime for different values of the scan number $N$. It should be noted that the average estimate of the dissipation rate $\varepsilon$ obtained from the same lidar data is independent of tabulated $N$ and equal to $4.1\cdot 10^{-3}$ m$^2$/s$^3$. It follows from Table 1 that as the scan number increases, the estimates of the kinetic energy and the integral scale increase, and for $N > 30$ (measurement time longer than 30 min) the practically complete saturation takes place.

As to the estimates of the turbulence parameters from the nighttime measurement data in the considered period at a height of 200 m, then the averaged (for six-hour period) estimate of the kinetic energy increase linearly with an increase of $N$ from $E$ = 0.12 (m/s)$^2$ at $N$ = 10 to $E$ = 0.24 (m/s)$^2$ at $N$ = 60 (twofold increase). The similar increase is also observed for the estimate of the dissipation rate. At $N$ = 30, the average estimate $\varepsilon = 5.5\cdot 10^{-6}$ m$^2$/s$^3$. The integral scale of turbulence determined by Eq. (24) has unrealistically high values ($\sim$ 4 km), which indicates that the above method of lidar data processing is inapplicable to nighttime measurements above the atmospheric surface layer at stable temperature stratification. A possible reason is ignorance of nonstationarity of the average wind, including mesoscale processes (for example, internal gravity waves), at the very weak turbulence. Therefore, we restricted our consideration to the results of lidar measurements of turbulence only in the zone of intense mixing, which occurred in daytime. During the experiment, the intense mixing in the entire layer up to 500 m was observed approximately from 10:30 to 19:00 (7/21/2016), from 11:00 to 20:00 (7/22/2016), and from 11:30 to 18:00 (7/23/2016) LT (Smalikho and Banakh, 2017).

Figure 6 exemplifies the data of lidar measurements at different height. The value of $M^{-1}\sum_{m=0}^{M-1}[<V_{\mathrm{L}}(\theta_m, R_k)> - \mathbf{S}(\theta_m)\cdot <\mathbf{V}(h_k)>]^2$ is smaller than $\bar{\sigma}_{\mathrm{L}}^2$ at least by factor 10. The blue curves in Figs.6 (b, d) were obtained with the use of smoothing averaging over three points (azimuth angles). It can be seen that at negative values of the average radial velocity $<V_{\mathrm{L}}(\theta_m, R_k)>$ (or $\mathbf{S}(\theta_m)\cdot <\mathbf{V}(h_k)>$) the variances of the lidar estimate of the radial velocity

$\sigma_{\mathrm{L}}^2(\theta_m, h_k)$ mostly exceed the corresponding variances at the positive values of the average radial velocity. As a result, the estimates of the along-wind momentum flux $<uw>$ determined by Eq. (25) (real part) are negative, as expected (Lumley and Panofsky, 1964; Monin and Yaglom, 1971; Byzova et al., 1989; Eberhard et al., 1989; Sathe et al., 2015).

All our results of spatiotemporal visualization of the average wind, turbulence parameters, and instrumental error in estimation of the radial velocity from lidar measurements on July 22 of 2016 in the period under consideration are shown in Fig. 7. Analogous results of estimation of the turbulence parameters were also obtained from lidar measurements on July 21 and 23 of 2016 in the above periods, but on July 23 the wind velocity $U$ was, on average, 1.8 times smaller than that on July 22, while the kinetic energy $E$ was 2 to 2.5 times smaller, and the dissipation rate $\varepsilon$ was 2.5 to 4 times smaller (Smalikho and Banakh, 2017). At the same time, the estimates of the integral scale $L_V$ were, on average, close to each other (maximum deviation is around 20%).

For illustration, Figs. 8 and 9 show, respectively, the time and height profiles of the wind turbulence parameters and the instrumental error in estimation of the radial velocity. The results presented for $\varepsilon$, $E$, $L_V$, $<uw>$, and $<vw>$ do not contradict the theory of the atmospheric boundary layer and quite correspond to the known experimental data for similar atmospheric conditions (Lumley and Panofsky, 1964; Monin and Yaglom, 1971; Byzova et al., 1989). The instrumental error in estimation of the radial velocity $\sigma_e$ depends mostly on the signal-to-noise ratio $\mathrm{SNR}$ : the higher $\mathrm{SNR}$ , the smaller $\sigma_e$. Since the probing radiation was focused to a distance of 500 m, $\sigma_e$ took the smallest values in the layer of 200 - 300 m. The error $\sigma_e$ plays an important role in fulfillment of condition (22), when turbulence is very weak. A necessary condition for obtaining the information about the turbulence energy dissipation rate $\varepsilon$ from lidar data with the use of Eq. (21) is fulfillment of the inequality $R'\psi_l << L_V$. In our case, for heights of 100, 300, and 500 m at $l$ = 3, the separation between the centers of the sensing volumes $R'\psi_3$ is equal, respectively, to 22, 67, and 111 m. According to the data of Fig. 7(d) and Fig. 8(d), this condition is true, that is, the dissipation rate is actually determined within the inertial subrange of turbulence.

Under the condition $L_V >> \max\{\Delta z, \Delta y_k\}$, in accordance with Eq.(16), the estimate of the kinetic energy of turbulence can be represented as $E = (3/2)[\bar{\sigma}_{\mathrm{L}}^2 - \sigma_e^2 + \sigma_t^2]$, where the instrumental error in estimating the radial velocity $\sigma_e$ and the turbulent broadening of the Doppler spectrum $\sigma_t^2$ are determined using Eqs. (23) and (17), respectively. If $\sigma_e^2$ and $\sigma_t^2$ are negligible, in comparison with the variance of the lidar estimate of the radial velocity $\bar{\sigma}_{\mathrm{L}}^2$, an estimate of the kinetic energy with a sufficiently high accuracy can be obtained using the equation: $E = (3/2)\bar{\sigma}_{\mathrm{L}}^2$. To study the effect of $\sigma_e^2$ and $\sigma_t^2$ on the estimation of the kinetic energy, we obtained vertical profiles of $E_1 = (3/2)\bar{\sigma}_{\mathrm{L}}^2$ , $E_2 = (3/2)[\bar{\sigma}_{\mathrm{L}}^2 - \sigma_e^2]$ and $E_3 = (3/2)[\bar{\sigma}_{\mathrm{L}}^2 - \sigma_e^2 + \sigma_t^2]$. Four examples of such profiles are shown in Fig. 10. It can be seen that the allowance of the instrumental error $\sigma_e$ is important in the layer above 400 m, where the $\sigma_e$ increases due to a decrease in the signal-to-noise ratio $\mathrm{SNR}$ (see Figures 6 (d), 7 (b) and 8 (b)). A comparison of the red and blue curves in Fig. 10 allows one to judge the effect of allowance of the spatial averaging of the radial velocity over the sensing volume on estimate of the turbulence kinetic energy. It follows from the data in Fig. 10 that the value $[(E_3 - E_2)/E_3]\times 100\%$ varies from 14% to 27% at a height of 100 m and from 10% to 16% at a height of 500 m. If for estimating the integral scale of turbulence $L_V$ in Eq. (24), instead of $E \equiv E_3$, to use $E_2$, then underestimation of the integral scale will be from 15% to 40%.

The estimation of the integral scale of turbulence $L_V$ by Eq. (24) with the coefficient $C_4$ = 0.38 assumes that the spatial structure of wind turbulence is described by the von Karman model. To clarify how close to reality is this assumption, we have compared the measured azimuth function $\bar{D}_{\mathrm{L}}(\psi_l) - 2\sigma_e^2$ with the function $D_a(\psi_l) = \varepsilon^{2/3} A(l\Delta y_k; L_V)$, where $A(l\Delta y_k; L_V)$ is calculated by Eq. (20), which takes into account the integral scale of turbulence $L_V$ through replacement of $\Phi(\kappa_1, \kappa_2)$ with

$$\Phi(\kappa_1,\kappa_2;L_V) = \frac{1}{3\pi}\frac{2C_1^2 C_2 L_V^{8/3}}{[1+(C_1 L_V)^2(\kappa_1^2+\kappa_2^2)]^{4/3}}\left[1+\frac{8}{3}\cdot\frac{(C_1 L_V \kappa_2)^2}{1+(C_1 L_V)^2(\kappa_1^2+\kappa_2^2)}\right]. \tag{27}$$

Equation (27) was derived in (Smalikho and Banakh, 2013) with the use of the von Karman model of isotropic turbulence. In calculations of $D_a(\psi_l) = \varepsilon^{2/3} A(l\Delta y_k; L_V)$, the experimentally obtained values of $\varepsilon$ (from $\bar{D}_{\mathrm{L}}(\psi_l)$ within the inertial subrange of turbulence) and $L_V$ (with the use of Eq. (24)) are used. We have also calculated the degree of deviation of the structure functions $\gamma$ by Eq. (11), where $D_r(l\Delta\theta)$ and $D_\perp(R' l\Delta\theta)$ were substituted with $\bar{D}_{\mathrm{L}}(\psi_l) - 2\sigma_e^2$ and $D_a(\psi_l)$, respectively.

Figure 11(a) depicts the spatiotemporal distribution of the parameter $\gamma$. According to this figure, the degree of deviation of the structure functions $\gamma$ varies from 0.014 to 0.22 (on average, about 0.1). The widest deviations are observed in the period from 12:30 to 14:30, when the lidar measurements were carried out under convective conditions of the atmospheric boundary layer. Figure 12 exemplifies the comparison of the structure functions $\bar{D}_{\mathrm{L}}(\psi_l)$, $\bar{D}_{\mathrm{L}}(\psi_l) - 2\sigma_e^2$, and $D_a(\psi_l)$. The last example demonstrates the importance of consideration of the instrumental error of the radial velocity in estimation of wind turbulence parameters $\varepsilon$, $E$ и $L_V$. Figures 11(a) and 12 suggest that Eq. (24) with $C_4$ = 0.38 (von Karman model) is applicable to estimation of the integral scale $L_V$. Since turbulence is anisotropic, the estimated integral scale $L_V$ should be considered as the integral scale of turbulence averaged over the azimuth angles of conical scanning at an elevation angle of 35.3°.

To calculate the error of lidar estimates of the dissipation rate, kinetic energy, and the integral scale of turbulence, we used the algorithm of numerical simulation, whose description can be found in papers of Smalikho and Banakh (2013) and Smalikho et al. (2013). In the numerical simulation, we set the input parameters $U$, $\sigma_e$, $\varepsilon$, $E$, and $L_V$ obtained from the lidar experiment. In addition, we assumed the stationarity and statistical homogeneity of the wind field and isotropy of turbulence. Figure 11(b) shows the spatiotemporal distribution of the relative error of lidar estimate of the turbulence energy dissipation rate. The error varies from 6.5% to 15%. Figure 13 shows the time series and height profiles of the relative error of estimation of the dissipation rate. It can be seen that for the conditions of this experiment we have the rather high accuracy of determination of the dissipation rate from data of the conically scanning Stream Line lidar. Thus, in the layer of 100 – 350 m, the relative error does not exceed 7.5%. Worsening of the accuracy of estimation of the dissipation rate with height is caused by an increase of the instrumental error $\sigma_e$ and a decrease of the dissipation rate $\varepsilon$. It is shown in Section 4 that from lidar data measured for four scans it is possible to obtain the estimate of the dissipation rate with a relative error of 20%. The results presented in this section were obtained from the data of 30 scans. In the case of stationary conditions, an increase in the scan number from 4 to 30 should lead to a decrease of the error from 20% to approximately 7% ( $\sqrt{30/4}$ times), which corresponds to the data of Figs. 11(b) and (13) up to a height ~ 350 m.

According to the results of numerical simulation for the experimental conditions considered in this section, the relative error of lidar estimate of the kinetic energy of turbulence varies insignificantly in the time and height ranges of Fig. 7(e) and averages about 10%. At the same time, the relative error of estimation of the integral scale of turbulence varies from 16% to 20% as a function of height and time. A reliable way to study capabilities of the considered method for estimation of the turbulence parameters is comparison of the results of simultaneous measurements by the lidar and the sonic anemometer at the same height.

Section 4 presents the results of simultaneous measurements of the dissipation rate $\varepsilon$ at a height of 43 m by the Stream Line lidar with conical scanning by the probing beam at the elevation angle $\varphi$ = 9° and the sonic anemometer installed at the tower (see Fig. 2). During the lidar measurements, whose results are presented above in Section 5, measurements by the sonic anemometer installed on the tower at a height of 43 m were carried out. Unfortunately, during these measurements the wind direction was so that the anemometer data were distorted due to wind flow around the tower. On August 27 of 2016, we again conducted joint measurements by the Stream Line lidar (the elevation angle $\varphi$ was also taken equal to 35.3°) and by the sonic anemometer, which measured raw data along the wind without distortions for 24 hours. Since the minimum distance of measurement by the Stream Line lidar is 120 – 150 m, it was impossible to conduct lidar measurements at the anemometer height of 43 m at this elevation angle. Taking into account that the kinetic energy $E$ varies more smoothly with height in comparison with other turbulent parameters $\varepsilon$ and $L_V$, we have compared the diurnal profiles of the kinetic energy obtained from joint measurements by the Stream Line lidar at a height of 100 m and by the sonic anemometer at a height of 43 m. The result of the comparison is shown in Fig. 14. Taking into account the difference in the measurement heights, we can say that a rather good agreement is observed between the time series of the kinetic energy of turbulence obtained from measurements by the different devices.

## 6 Conclusions

Thus, in this paper we have proposed a relatively simple method for determination of the turbulence energy dissipation rate, kinetic energy, and integral scale of turbulence from measurements by conically scanning PCDL. The method is applicable in the case that the longitudinal and transverse dimensions of the sensing volume do not exceed the integral scale of turbulence. Since the dissipation rate is estimated from the azimuth structure function within the inertial subrange of turbulence, it is sufficient to calculate the function $A(l\Delta y_k)$ for different heights $h_k$ by Eq. (20), and then with Eq. (21) it is possible to retrieve the vertical profiles $\varepsilon(h_k)$. In the estimation of the kinetic energy of turbulence, the spatial averaging of the radial velocity over the sensing volume is taken into account. For this purpose, it is necessary to calculate the function $F(\Delta y_k)$ by Eq. (19) and to use Eq. (16). Then, the integral scale of turbulence is determined with Eq. (24). In contrast to the approach described by Frehlich et al. (2006) and Smalikho and Banakh (2013), in this method it is not needed to calculate the azimuth structure function of the radial velocity averaged over the sensing volume with the use of the spectrum model in form (27) and to apply the procedure of least-square fitting of the calculated function to the measured one. As was shown in Section 2, this fitting in some cases can lead to the overestimation of the integral scale of turbulence. We have seen this, when applied this fitting to the lidar data of the experiment (measurements in the daytime) described in Section 5. As a result, we have obtained unrealistically high values for estimates of the integral scale of turbulence at low heights of 100–200 m. Sometimes such estimates exceed 1 km in contrast to results shown in Figures 6(f), 7(d) and 8(d).

The comparison of measurements of the turbulence energy dissipation rate by the Stream Line lidar with the method described in Section 3 and the data measured by the sonic anemometer has demonstrated a good agreement. The data of the lidar experiment of 2016 have been used to obtain the spatiotemporal distributions of different wind turbulence parameters with a height resolution of 10 m and a time resolution of 30 min. The lidar estimates of turbulence have been analyzed. It has been shown that the use of conical scanning during measurements by PCDL and the method for processing of lidar data proposed in this paper allows obtaining the information about wind turbulence in the atmospheric mixing layer with a rather high accuracy. However, as shown by the lidar experiment conducted under stable temperature stratification outside the layer of intensive turbulent mixing (Smalikho and Banakh, 2017), this method is not applicable and, consequently, further investigations and development of new approaches are needed.

**Appendix: List of symbols**

| | |
|---|---|
| $B_{\parallel}(r)$ | Longitudinal correlation function of wind velocity |
| $c$ | Speed of light |
| $C_K \approx 2$ | Kolmogorov constant |
| $C_1 = 8.4134$ | |
| $C_2 = 1.2717$ | |

$C_3 = 0.0652$

$C_4 = 0.3796$

$D_r(\psi;\theta)$ Azimuth structure function of the radial velocity

$D_r(\psi)$ Azimuth structure function of the radial velocity for isotropic turbulence

$\bar{D}_r(\psi)$ Averaged azimuth structure function of the radial velocity (Eq.(5))

$\bar{D}_{\mathrm{L}}(\psi_l)$ Azimuth structure function of lidar estimate of the radial velocity

$\bar{D}_a(\psi_l)$ Azimuth structure function of the radial velocity averaged over the sensing volume

$D_\perp(y')$ Transverse structure function of wind velocity

$E = (\sigma_w^2 + \sigma_u^2 + \sigma_v^2)/2$ Kinetic energy of turbulence

$f_p$ Pulse repetition frequency

$L_V$ Integral scale of turbulence

$l_V$ Inner scale of turbulence

$N$ Number of conical scans

$N_a$ Number of probing pulses used for the accumulation

$R$ Range (distance from lidar)

$R_0$ Minimum range

$R' = R\cos\varphi$ Radius of the circle along which the sensing volume moves during the conical scanning

$r_H$ Scale of the low-frequency boundary of the inertial subrange

$S_\parallel(\kappa)$ Longitudinal spatial spectrum of wind velocity fluctuations

$S_\perp(\kappa)$ Transverse spatial spectrum of wind velocity fluctuations

SNR Signal-to-noise ratio

$T_{\mathrm{scan}}$ Duration of one conical scan

$T_W$ Temporal window width

$u$ Fluctuations of longitudinal wind component

$U$ Average wind velocity

$<uw>$ Along-wind momentum flux

$v$ Fluctuations of transverse wind component

$\mathbf{V} = \{V_z, V_x, V_y\}$ Wind vector, where $V_z$ is the vertical component, $V_x$ and $V_y$ are the horizontal components

$V_a$ Radial velocity averaged over the sensing volume

| | |
|---|---|
| $V_e$ | Random instrumental error of unbiased estimate of the radial velocity |
| $V_{\mathrm{L}}$ | Lidar estimate of the radial velocity |
| $V_r$ | Radial velocity |
| $< vw >$ | Cross-wind component of momentum flux |
| $w$ | Fluctuations of vertical wind component |
| $\gamma$ | Parameter characterizing the degree of deviation of structure functions |
| $\Delta h = \Delta R \sin \varphi_E$ | Vertical resolution |
| $\Delta R$ | Range gate length |
| $\Delta y_k = \Delta\theta R_k \cos\varphi$ | Transverse size of the sensing volume at distance $R_k$ from the lidar |
| $\Delta z$ | Longitudinal size of the sensing volume |
| $\Delta\theta$ | Azimuth angle resolution |
| $\varepsilon$ | Turbulent energy dissipation rate |
| $\varepsilon_{\mathrm{L}}$ | Estimate of the turbulent energy dissipation rate from measurement by lidar |
| $\varepsilon_{\mathrm{S}}$ | Estimate of the turbulent energy dissipation rate from measurement by sonic anemometer |
| $\theta$ | Azimuth angle |
| $\theta_V$ | Average wind direction angle |
| $\sigma_a^2 = < V_a^2 > - < V_a >^2$ | Variance of radial velocity averaged over the sensing volume |
| $\sigma_e^2 = < V_e^2 >$ | Variance of random instrumental error of unbiased estimate of the radial velocity |
| $\sigma_e$ | Instrumental error of radial velocity estimate |
| $\sigma_{\mathrm{L}}^2 = < V_{\mathrm{L}}^2 > - < V_{\mathrm{L}} >^2$ | Variance of lidar estimate of radial velocity |
| $\sigma_p$ | Duration of the probing pulse determined by the $e^{-1}$ power level |
| $\sigma_r^2 = < V_r^2 > - < V_r >^2$ | Variance of the radial velocity |
| $\bar{\sigma}_r^2$ | Variance of the radial velocity after averaging over azimuth angles interval [0°, 360°] |
| $\sigma_t^2 = \sigma_r^2 - \sigma_a^2$ | Turbulent broadening of the Doppler spectrum |
| $\sigma_u^2 = < u^2 >$ | Variance of longitudinal wind component |
| $\sigma_v^2 = < v^2 >$ | Variance of transverse wind component |
| $\sigma_w^2 = < w^2 >$ | Variance of vertical wind component |
| $\bar{\sigma}_\alpha^2 = M^{-1} \sum_{m=0}^{M-1} \sigma_\alpha^2(\theta_m)$ | Variance $\sigma_\alpha^2$ averaged over azimuth angles interval [0°, 360°], where subscripts $\alpha$ means L or $a$ |

| | |
|---|---|
| $\varphi$ | Elevation angle |
| $\varphi_E$ | Elevation angle equal to 35.3° |
| $\omega_s$ | Angular rate of conical scanning |

*Acknowledgements*. The authors are grateful to colleagues from the Institute of Atmospheric Optics SB RAS A.V. Falits, Yu.A. Rudi, and E.V. Gordeev for the help in experiments.

This study was supported by the Russian Science Foundation, Project No. 14-17-00386-П.

**References**

Banakh, V. and Smalikho, I.: Coherent Doppler Wind Lidars in a Turbulent Atmosphere, Artech House Publishers, ISBN-13: 978-1-60807-667-3, 2013.

Banakh, V. A., Smalikho, I. N., Falits, A. V., Belan, B. D., Arshinov, M. Yu., and Antokhin, P. N.: Joint radiosonde and Doppler lidar measurements of wind in the boundary layer of the atmosphere, Atmos. Ocean. Optics., 28, 185-191, doi:10.1134/S1024856015020025, 2015.

Banakh, V. A. and Smalikho, I. N.: Lidar observations of atmospheric internal waves in the boundary layer of atmosphere on the coast of Lake Baikal, Atmos. Meas. Tech., 9, 5239-5248, doi:10.5194/amt-9-5239-2016, 2016.

Banta, R. M., Pichugina, Y. L., and Brewer, W. A.: Turbulent velocity-variance profiles in the stable boundary layer generated by a nocturnal low-level jet, J. Atmos. Sci., 63, 2700–2719, doi: http://dx.doi.org/10.1175/JAS3776.1, 2006.

Byzova, N.L., Ivanov, V.N., and Garger, E.K.: Turbulence in Atmospheric Boundary Layer, Gidrometeoizdat, Leningrad, 265 pp. ISBN 5-286-00151-3, 1989. [in Russian].

Davies, F., Collier, C. G., Pearson, G. N., and Bozier, K. E.: Doppler lidar measurements of turbulent structure function over an urban area J. Atmos. Ocean. Tech., 21, 753-761, doi:10.1175/1520-0426(2004)021<0753:DLMOTS>2.0.CO;2, 2004.

Eberhard, W. L., Cupp, R. E., and Healy, K. R.: Doppler lidar measurement of profiles of turbulence and momentum flux, J. Atmos. Ocean. Tech., 6, 809–819, doi: 10.1175/1520-0426(1989)006<0820:AOADLM>2.0.CO;2, 1989.

Frehlich, R. G., Hannon, S.M., and Henderson, S.W.: Coherent Doppler lidar measurements of wind field statistics, Boundary-Layer Meteorology, 86, 223-256, doi:10.1023/A:1000676021745,1998.

Frehlich, R. G. and Cornman, L.B.: Estimating spatial velocity statistics with coherent Doppler lidar, J. Atmos. Ocean. Tech., 19, 355-366, doi:10.1175/1520-0426-19.3.355, 2002.

Frehlich, R.G., Meillier, Y., Jensen, M. L., Balsley, B., and Sharman, R.: Measurements of boundary layer profiles in urban environment, J. Appl. Meteorol. and Climatol., 45, 821-837, doi:10.1175/JAM2368.1, 2006.

Gal-Chen, T., Xu, M., and Eberhard, W. L.: Estimations of atmospheric boundary layer fluxes and other turbulence parameters from Doppler lidar data, J. Geophys. Res. 97, 409–418, doi:10.1029/91JD03174, 1992.

Kolmogorov, A.N.: Local structure of turbulence in incompressible viscous fluid at very large Reynolds numbers, Doklady AN SSSR, 30, 299-303б 1941.

Lumley, J. L. and Panofsky, H. A.: The Structure of Atmospheric Turbulence, New York (Interscience Publishers), 1964.

Monin, A. S., and Yaglom, A. M.: Statistical Fluid Mechanics, Volume II: Mechanics of Turbulence, M.I.T. Press, Cambridge, Mass., 1971.

O'Connor, E. J., Illingworth, A. J., Brooks, I. M., Westbrook, C. D., Hogan R. J., Davies, F., and Brooks, B. J.: A method for estimating the kinetic energy dissipation rate from a vertically pointing Doppler lidar, and independent evaluation from balloon-borne in situ measurements, J. Atmos. Ocean. Tech., 27, 1652 -1664, doi:10.1175/2010JTECHA1455.1, 2010.

Pearson, G., Davies, F., and Collier, C.: An analysis of performance of the UFAM pulsed Doppler lidar for the observing the boundary layer, J. Atmos. Ocean. Tech., 26, 240-250, doi:10.1175/2008JTECHA1128.1, 2009.

Sathe, A. and Mann, J.: A review of turbulence measurements using ground-based wind lidars, Atmos. Meas. Tech., 6, 3147–3167, doi:10.5194/amt-6-3147-2013 , 2013.

Sathe, A., Mann, J., Vasiljevic, N., and Lea, G.: A six-beam method to measure turbulence statistics using ground-based wind lidars, Atmos. Meas. Tech., 8, 729–740, doi:10.5194/amt-8-729-2015, 2015.

Smalikho, I., Köpp F., and Rahm S.: Measurement of atmospheric turbulence by 2-micron Doppler lidar, J. Atmos. Ocean. Tech., 22, 1733-1747, doi:10.1175/JTECH1815.1, 2005.

Smalikho, I.N. and Banakh, V.A.: Accuracy of estimation of the turbulent energy dissipation rate from wind measurements with a conically scanning pulsed coherent Doppler lidar. Part I. Algorithm of data processing, Atmos. Ocean. Opt., 26, 404–410, doi:10.1134/S102485601305014X, 2013.

Smalikho, I.N. Banakh, V.A., Pichugina Y. L., and Brewer W. A.: Accuracy of estimation of the turbulent energy dissipation rate from wind measurements with a conically scanning pulsed coherent Doppler lidar. Part II. Numerical and atmospheric experiments, Atmos. Ocean. Opt., 26, 411–416, doi:10.1134/S1024856013050151, 2013.

Smalikho, I. N. and Banakh V. A.: Investigation of feasibility of wind turbulence measurement by a pulsed coherent Doppler lidar in the atmospheric boundary layer, Proceedings of 28th International Laser Radar Conference (25-30 June 2017, Bucharest, Romania) / 06 – Lidar applications in atmospheric dynamics and surface exchanges boundary layer, winds and turbulence / 061_293_I_Smalikho.pdf, 2017.

Vinnichenko, N. K., Pinus, N. Z., Shmeter, S. M., and Shur G. N.: Turbulence in the Free Atmosphere, edited by: Dutton, J. A., Consultants Bureau, 262 pp., ISBN-13: 978-1-4757-0100-5, 1973.

**Table 1**: Average estimates of the kinetic energy and the integral scale of turbulence as functions of the number of scans used during the lidar measurements in the period from 12:00 to 18:00 LT on 7/22/2016 at a height of 200 m.

| Scan number (or measurement duration in min) | 10 | 20 | 30 | 40 | 50 | 60 |
|---|---|---|---|---|---|---|
| Kinetic energy of turbulence, $(m/s)^2$ | 1.71 | 1.84 | 1.88 | 1.91 | 1.92 | 1.93 |
| Integral scale of turbulence, m | 208 | 231 | 239 | 244 | 247 | 249 |

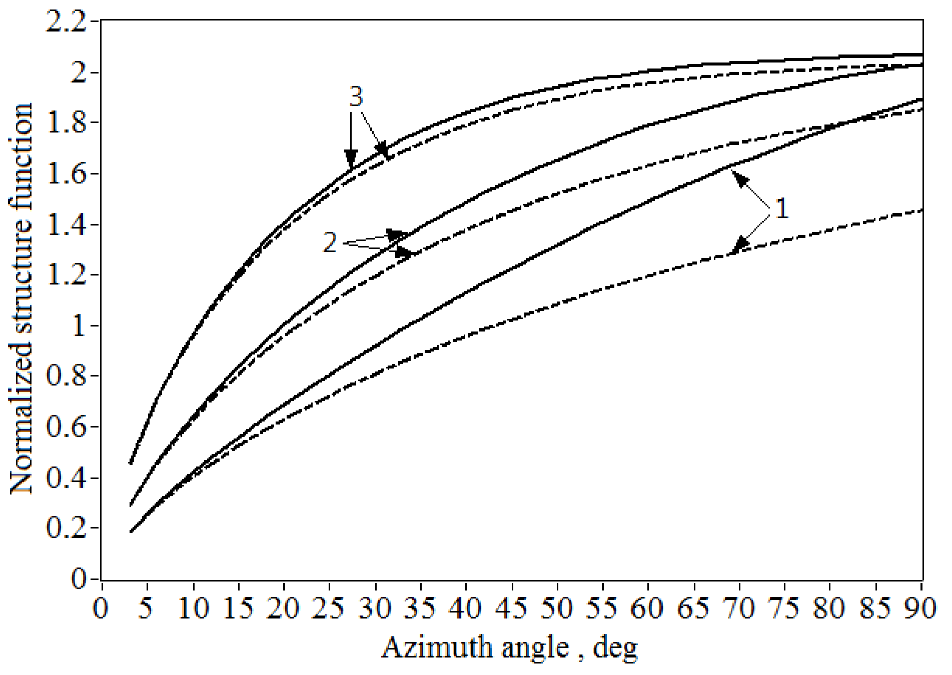


**Figure 1**: Normalized structure functions $D_r(\psi)/\sigma_r^2$ (solid curves) and $D_\perp(R'\psi)/\sigma_r^2$ (dashed curves) calculated, respectively, by Eq. (7) and (8) with the use of model (9) at $R'/L_V$ = 0.5 (curves 1), 1 (curves 2), and 2 (curves 3).

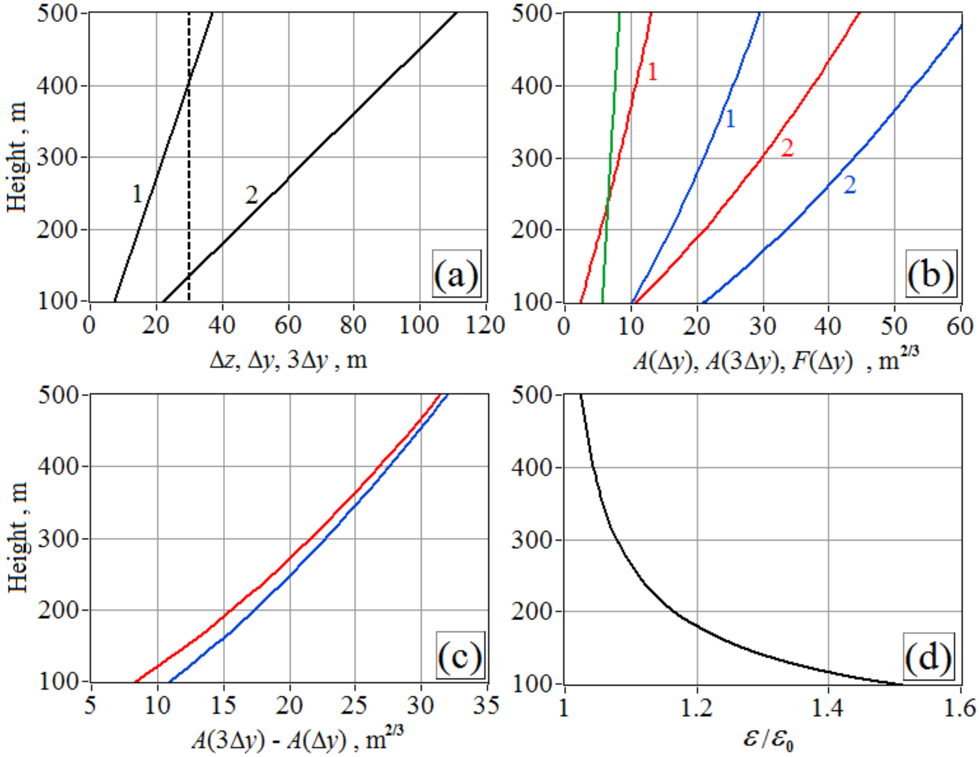


**Figure 2**: Vertical profiles of (a) longitudinal size of the sensing volume $\Delta z$ (dashed curve), transverse size of the sensing volume $\Delta y_k$ (curve 1) and $3\Delta y_k$ (curve 2); (b) $F(\Delta y_k)$ (green curve), $A(\Delta y_k)$ (red curve 1), $A_0(\Delta y_k)$ (blue curve 1), $A(3\Delta y_k)$ (red curve 2), $A_0(3\Delta y_k)$ (blue curve 2); (c) differences $A(3\Delta y_k)-A(\Delta y_k)$ (red curve) and $A_0(3\Delta y_k)-A_0(\Delta y_k)$ (blue curve); (d) ratio $\varepsilon/\varepsilon_0$.

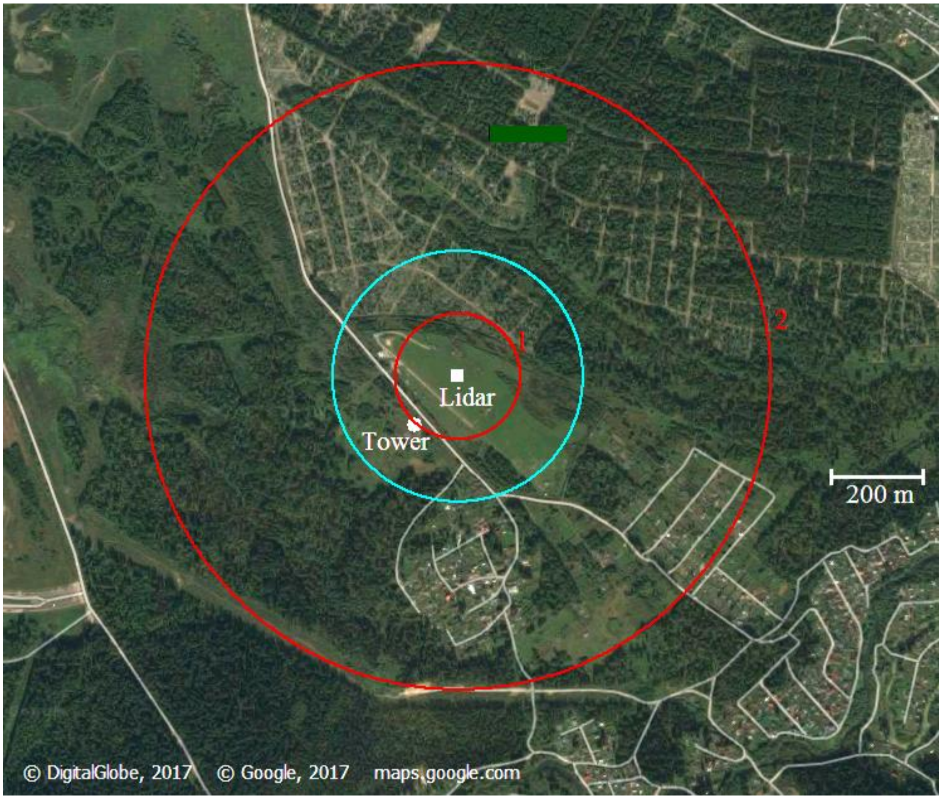


**Figure 3**: Map of the experimental site in 2014 and 2016. The blue circle shows the trajectory of the lidar sensing volume at a height of 43 m during the measurement at the elevation angle $\varphi = 9°$ in 2014. Red circles 1 and 2 shows the trajectories of the lidar sensing volume at heights of, respectively, 100 and 500 m during the measurement at $\varphi = 35.3°$ in 2016. Coordinates of the lidar point were 56°28'51.41"N, 85°06'03.22"E.

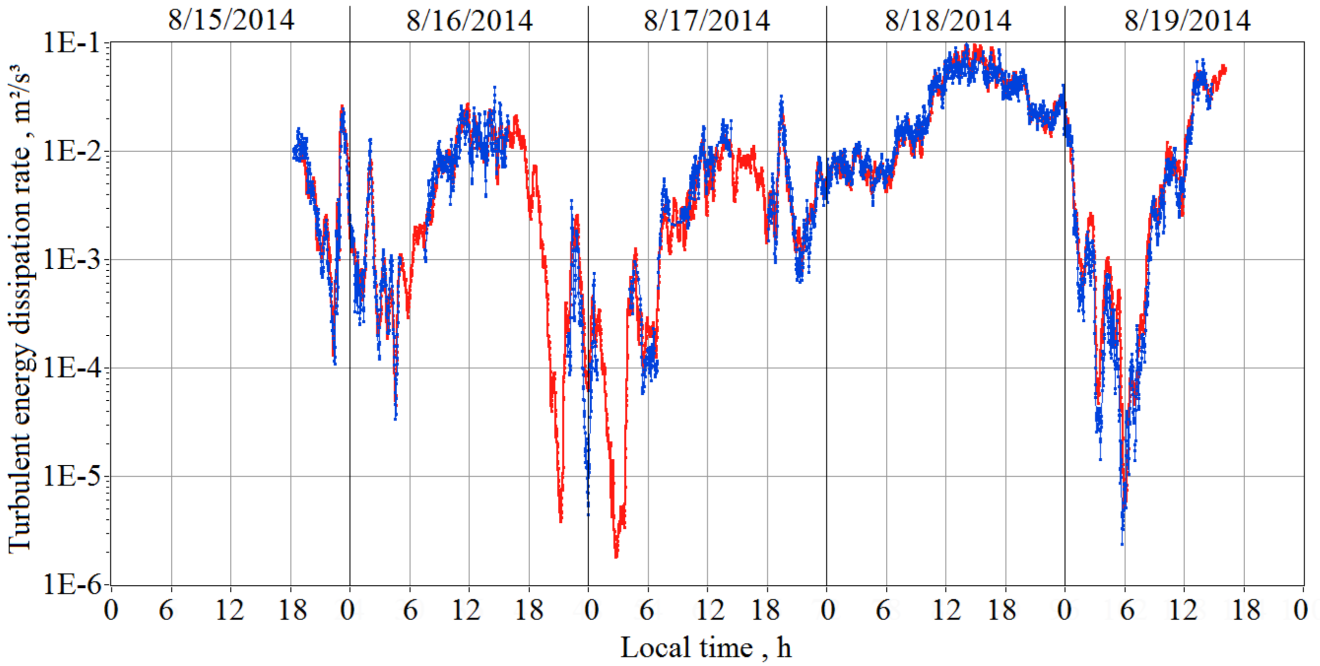


**Figure 4**: Time series of the turbulence energy dissipation rate obtained from measurements by the sonic anemometer (red curve) and the Stream Line lidar (blue curves) at a height of 43 m.

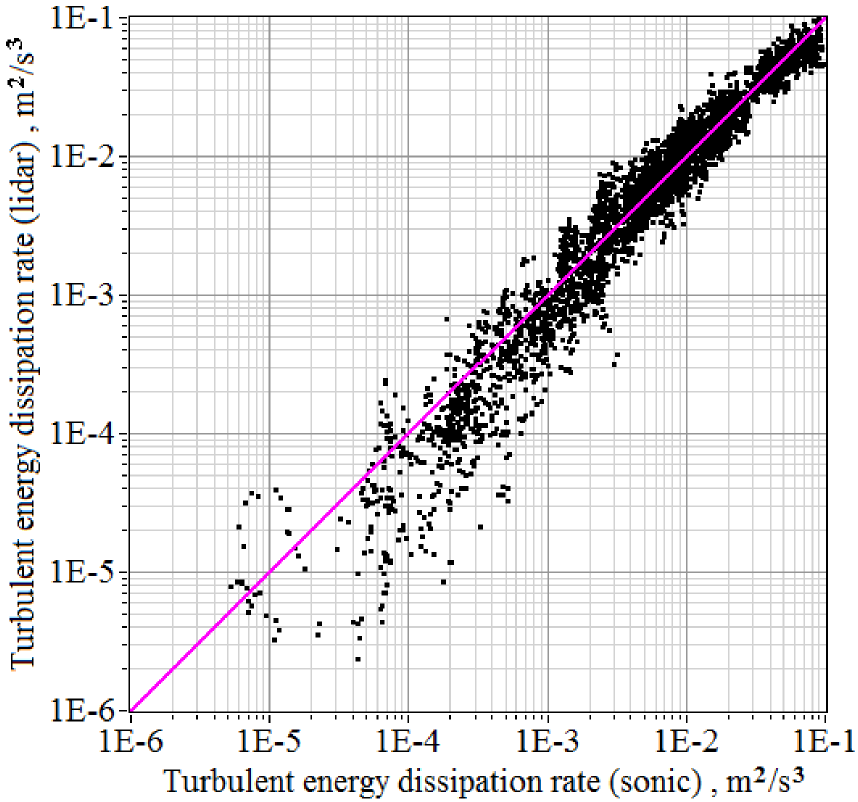


**Figure 5**: Comparison of estimates of the turbulence energy dissipation rate obtained from data of simultaneous measurements by the sonic anemometer and the Stream Line lidar. Time series of these estimates are shown in Fig.3.

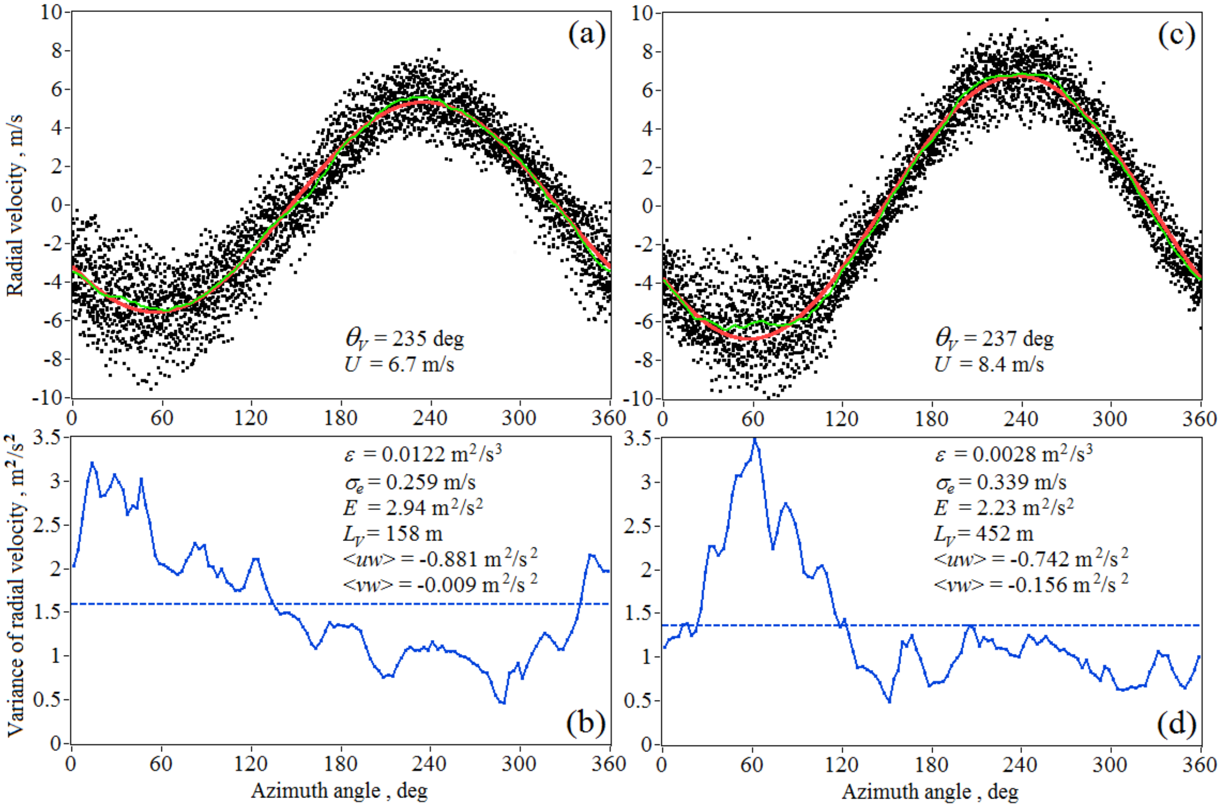


**Figure 6**: Single estimates of the radial velocity $V_{\mathrm{L}}(\theta_m, R_k, n)$ (dots); radial velocity averaged over 30 scans, $<V_{\mathrm{L}}(\theta_m, R_k)>$ (green curves); radial velocities as a result of sine-wave fitting, $V_{\mathrm{L}}(\theta_m, R_k) = \mathbf{S}(\theta_m)\cdot <\mathbf{V}(h_k)>$ (red curves) [(a), (c)] and variances of lidar estimate of the radial velocity $\sigma_{\mathrm{L}}^2(\theta_m, h_k)$ (blue curves) [(b), (d)] as functions of the azimuth angle $\theta_m$ obtained from measurements by the Stream Line lidar on 7/22/2016 from 14:09 to 14:39 LT at the heights $h_k = R_k \sin\varphi_E$ = 109 m [(a), (b)] and 504 m [(c), (d)]. Dashed curves show the variance averaged over the azimuth angle and the lidar estimate of the radial velocity $\bar{\sigma}_{\mathrm{L}}^2$.

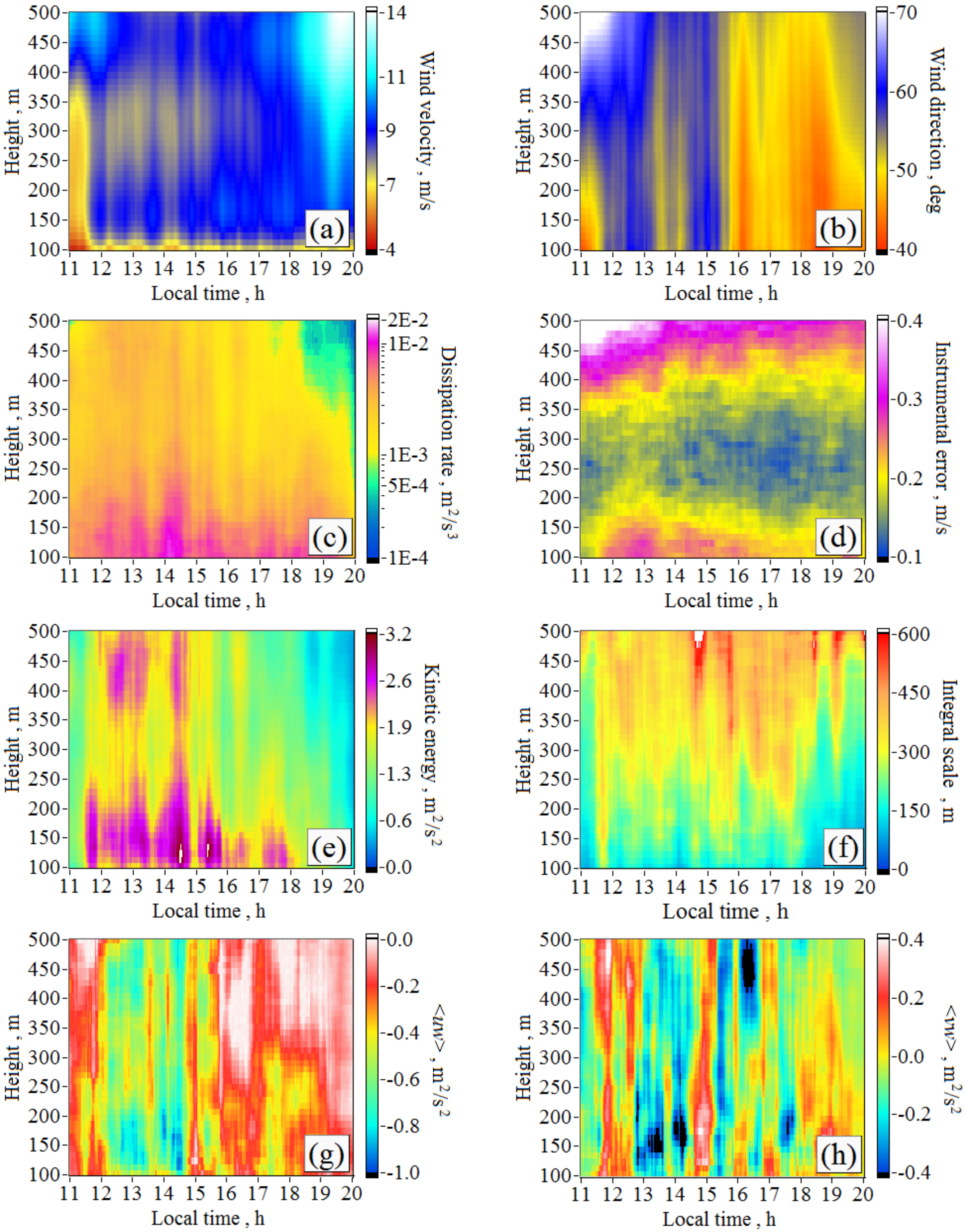


**Figure 7**: Spatiotemporal distributions of the average wind velocity $U$ (a), wind direction angle $\theta_V$ (b), turbulent energy dissipation rate $\varepsilon$ (c), instrumental error of estimation of the radial velocity $\sigma_e$ (d), kinetic energy of turbulence $E$ (e), integral scale of turbulence $L_V$ (f), and momentum fluxes $<uw>$ (g) and $<vw>$ (h) obtained from measurements by the Stream Line lidar on 7/22/2016.

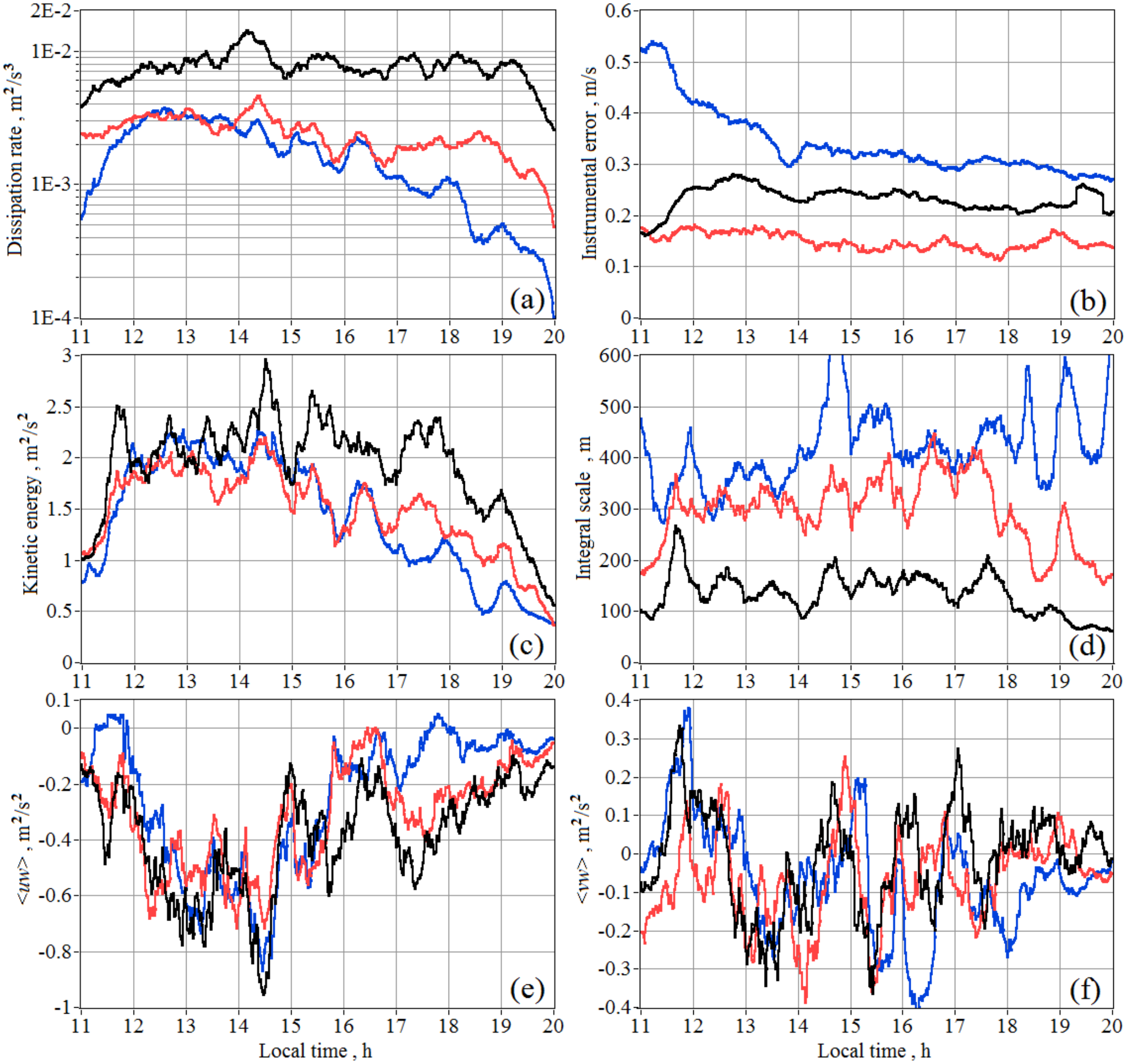


**Figure 8**: Temporal series of the turbulent energy dissipation rate $\varepsilon$ (a), instrumental error of radial velocity $\sigma_e$ (b), kinetic energy of turbulence $E$ (c), integral scale of turbulence $L_V$ (d), momentum fluxes $<uw>$ (e) and $<vw>$ (f) at heights of 100 m (black curves), 300 m (red curves), and 500 m (blue curves) taken from data of Fig. 6.

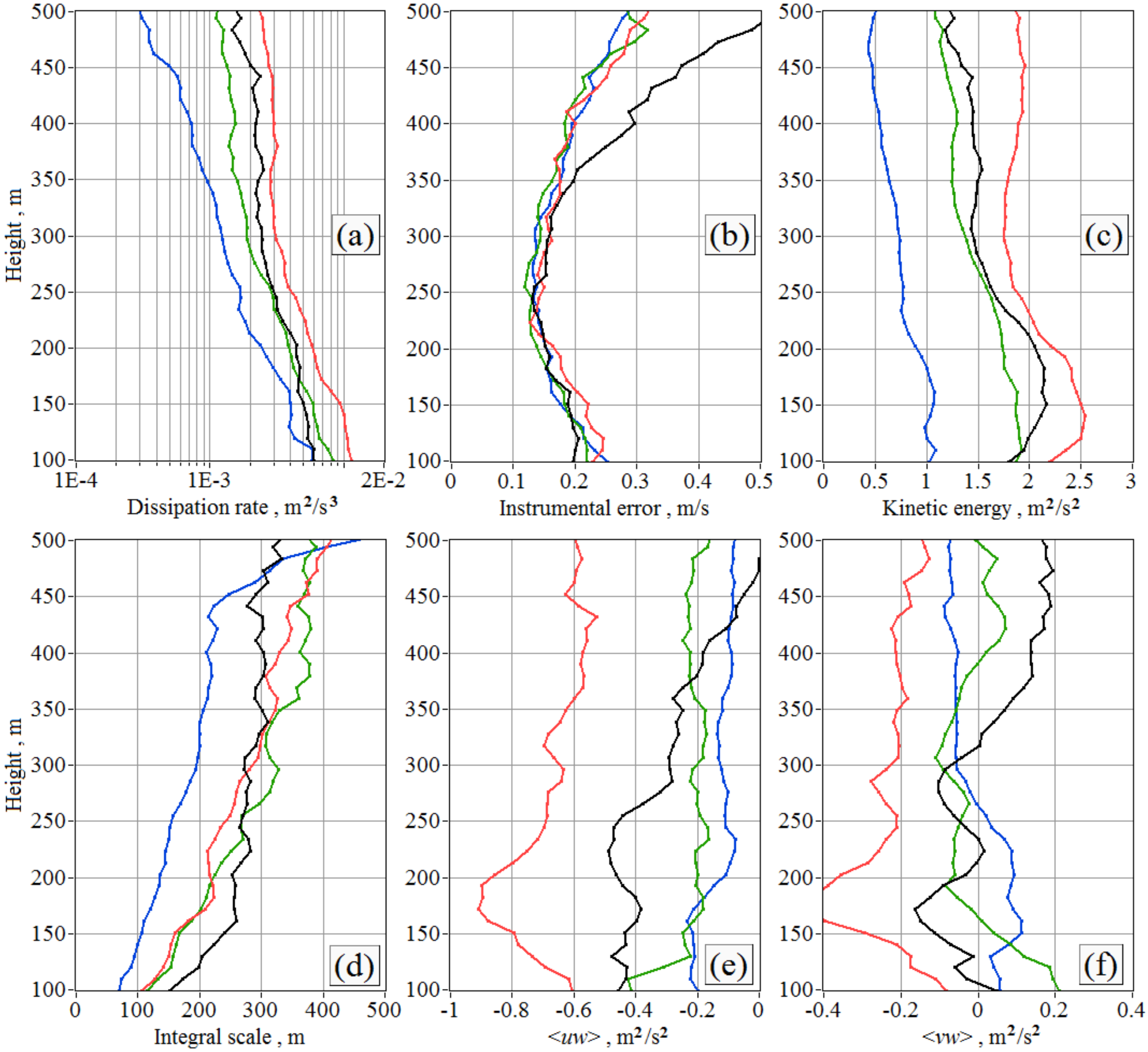


**Figure 9**: Vertical profiles of the turbulent energy dissipation rate $\varepsilon$ (a), instrumental error of radial velocity estimate $\sigma_e$ (b), kinetic energy of turbulence $E$ (c), integral scale of turbulence $L_V$ (d), momentum fluxes $<uw>$ (e) and $<vw>$ (f) at 11:30 (black curves), 14:00 (red curves), 17:00 (green curves), and 19:30 (blue curves) taken from the data of Fig. 6.

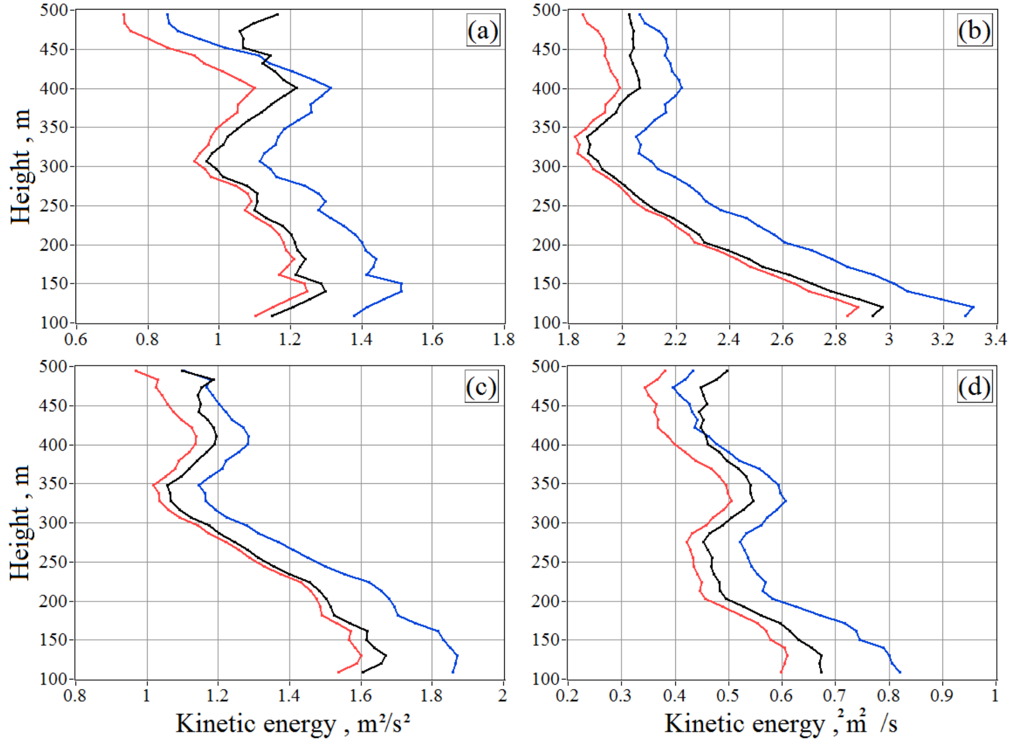


**Figure 10**: Vertical profiles of the turbulence kinetic energy estimates as $E_1 = (3/2)\bar{\sigma}_{\mathrm{L}}^2$ (black curves), $E_2 = (3/2)[\bar{\sigma}_{\mathrm{L}}^2 - \sigma_e^2]$ (red curves), and $E_3 = (3/2)[\bar{\sigma}_{\mathrm{L}}^2 - \sigma_e^2 + \sigma_t^2]$ (blue curves) obtained from measurements by stream Line lidar on 7/29/2016 at 11:17 (a), 14:31 (b), 16;55 (c), and 19:47 (d) of LT.

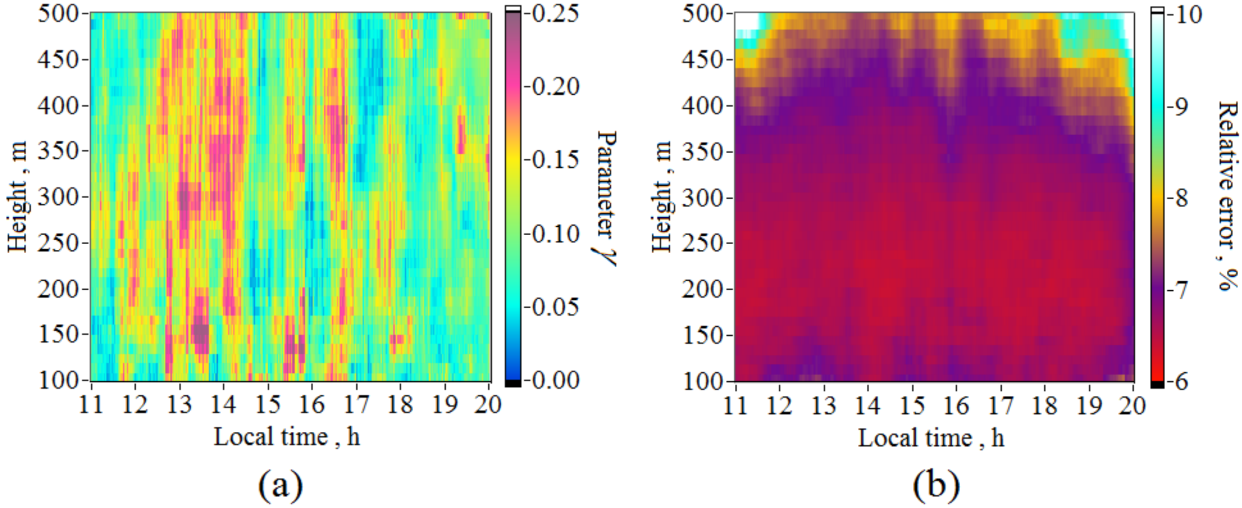


**Figure 11**: Time-height plots of the parameter $\gamma$ (a) and the relative error of estimation of the dissipation rate (b) obtained from measurements by the Stream Line lidar on 7/22/2016.

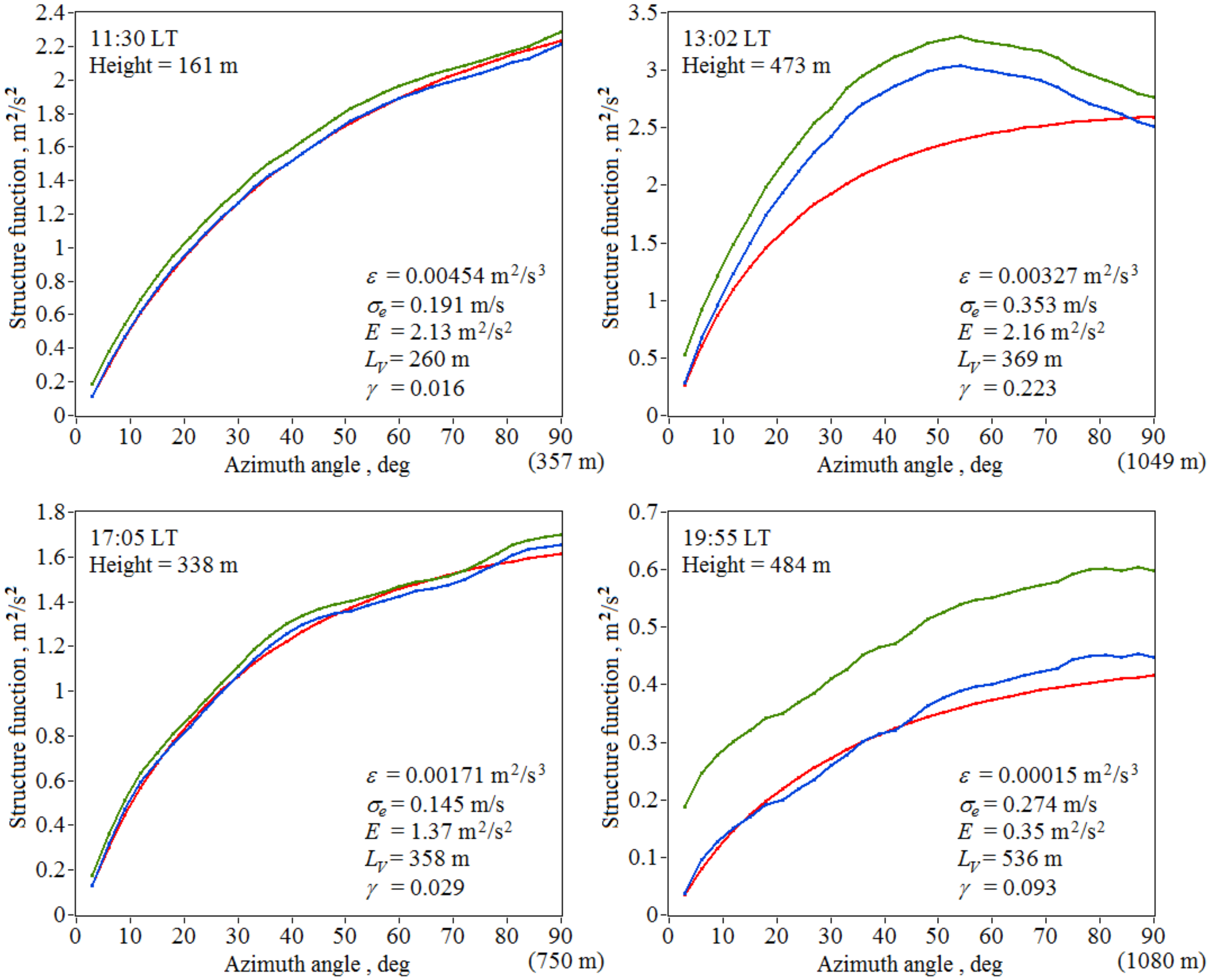


**Figure 12**: Examples of the azimuth structure functions $\bar{D}_{\mathrm{L}}(\psi_l)$ (green curves), $\bar{D}_{\mathrm{L}}(\psi_l)-2\sigma_e^2$ (blue curves), and $D_a(\psi_l)$ (red curves) obtained from measurements by the Stream Line lidar on 7/22/2016. The functions $D_a(\psi_l)$ were calculated by Eqs. (17), (19), and (23) with the use of experimental values of $\varepsilon$ and $L_V$. The arc length in the base of the scanning cone $y_k=(\pi/180^{\mathrm{o}})\psi_l\, h_k/\tan\varphi_E$ at $\psi_l$ = 90° is given in parenthesis.

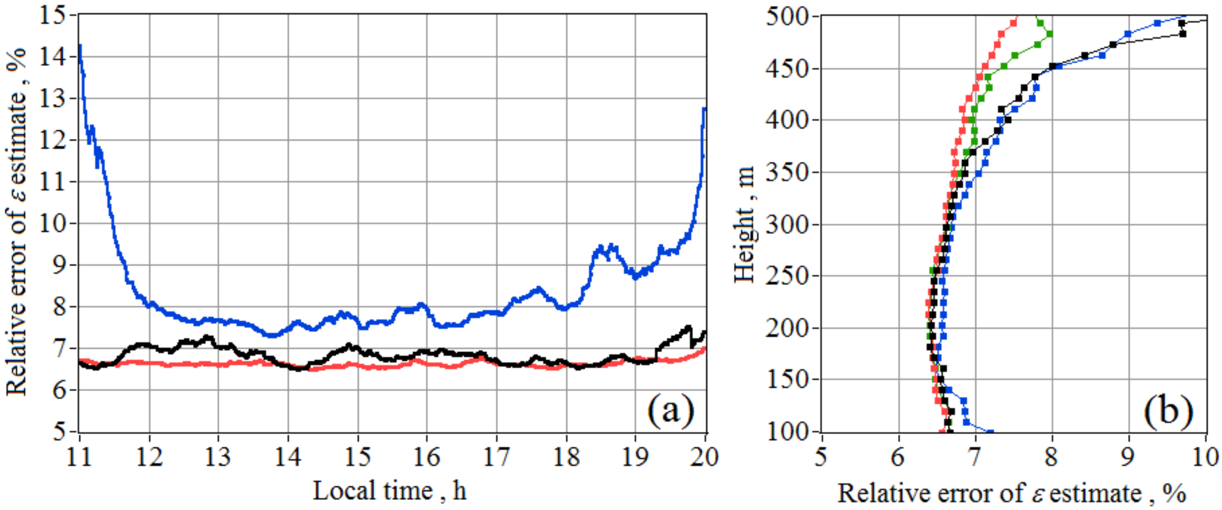


**Figure 13**: Time series of the relative error of estimation of the turbulence energy dissipation rate (a) at heights of 100 m (black curve), 300 m (red curve), and 500 m (blue curve) and height profiles of the relative error of estimation of the turbulence energy dissipation rate (b) at 11:30 (black squares), 14:00 (red squares), 17:00 (green squares), and 19:30 (blue squares) calculated from data of Fig. 8 (a,b).

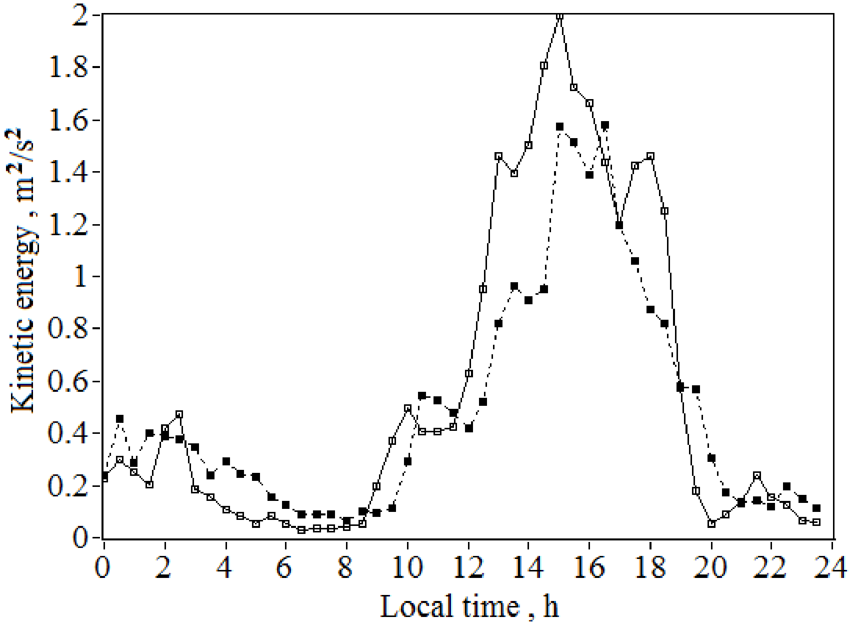


**Figure 14**: Diurnal profiles of the kinetic energy of turbulence obtained from simultaneous measurements by the sonic anemometer at a height of 43 m (squares connected by solid lines) and the Stream Line lidar at a height of 100 m (squares connected by dashed lines) on 8/27/2016.

## Responses for the reviewers of the manuscript

We thank very much the reviewers for their time and efforts, thoughtful and very useful comments. We have incorporated most of their suggested revisions as indicated below.

**Referee #1**

In this manuscript, the authors describe how various turbulent parameters can be measured with a continuously conically scanning Doppler lidar. The techniques for measurement of the parameters are described in detail, and sample results of the measurements are shown. Doppler lidar measurements of the dissipation rate are compared with a sonic anemometer at 43 m, and are shown to generally agree well, except with some low biases under stable conditions when the lidar is unable to resolve the any portion of the inertial subrange. The turbulence kinetic energy from the Doppler lidar is shown to generally agree with measurements from a sonic anemometer at a lower height. In all, the scientific quality of the manuscript appears to be solidly based in theory and good. The work builds on previous work, with new refinements made to the strategy. However, there are a few areas of the manuscript that could be clarified, as sections of the text are difficult to follow. As such, I recommend this manuscript be suitable for publication in AMT after minor revisions, in which the following comments, which are mostly of clarification, are addressed.

Specific Comments:

a) P. 1, line 19; p. 2, line 5 (and elsewhere): Change 'raw lidar data' to 'radial velocities'. By 'raw data', I interpret that to be the measured Doppler spectrum, which are not used directly in the referenced techniques to measure turbulence.

The phrase "raw data measured" has been replaced by "measurements".

b) p. 2, line 9: By 'averaging over the sensing volume', clarify that you mean the spatial-temporal averaging of the pulse length over one beam accumulation and not the averaging over the entire conical area.

Page 2, line 9: "(see Eq.(6) in paper of Smalikho and Banakh, 2013)" has been added.

c) p. 2 line 12: What are dr and σr?

Page 2, line 13: "and $\sigma_r^2 = B_{||}(0)$ is the variance" and "radial" have been added.

"dr" is an infinitesimal increment of the integration variable "r" (separation between two points).

d) p. 2 line 20: Quantify 'high spatial resolution'.

Page 2, lines 21-22: "(longitudinal size of the sensing volume can be around 30 m)" has been added.

e) p. 2 line 23: What disadvantages of the earlier methods, precisely? The averaging over the sensing volume?

We do not know publications in which authors would take into account the effect of averaging of the radial velocity over the sensing volume when estimating the kinetic energy of turbulence.

f) p. 2 line 24: Change 'spatiotemporal' to 'time and height'. The term 'spatiotemporal' is too general, and generally means that information on the horizontal variability is measured/known.

Fixed.

g) p. 6 lines 22-24: This section is difficult to follow. Providing more text to describe the different terms and how they are related would be helpful.

Text on page 6 (lines 18-24) of initial version of the manuscript has been replaced by the text on page 6 (lines 19-26) and page 7 (lines 1-3) of the revised manuscript.
Page 7, line 13: "(Banakh and Smalikho, 2013)" has been added.

h) p. 7-8: For this section in particular, it would be helpful to add a figure providing a few examples of the 2-dimensional spectrum and showing how the different parameters are calculated from it (particularly interested in σe, σt), including adding a paragraph discussing the figures. This would be similar to showing how different parameters are calculated in Fig. 5.

Page 9, lines 3-13: The paragraph "With increasing range … without taking into account the averaging of the radial velocity over the sensing volume." has been added.
Page 9, lines 14-26: The paragraph "Figure 2 shows vertical profiles … the underestimation does not exceed 5%." has been added.
Page 24: Figure 2 has been added.
The sentence "The analysis of results for the kinetic energy of turbulence … is understated by 10 - 20%, especially, in the layer up to 200 m." (page 13, lines 9-12 in the initial variant of the manuscript) has been removed.
Page 14, lines 22-30 and page 15, lines 1-4: The paragraph "Under the condition … then underestimation of the integral scale will be from 15% to 40%." has been added.
Page 32: Figure 10 has been added.

i) p. 10 line 10: How much of the data was unusable exactly? The percentage of unusable data would be helpful.

Page 11, line 16: "(around 15%)" has been added.

j) p. 10 line 13: What was the averaging time that the results shown in Fig. 3 were computed over? Based on p. 9 lines 19/24, it seems that 4 PPIs were used (over 5 minutes) while the sonic anemometer used 20 min of data. How were these differences in averaging times rectified?

If the same measurement time is used for the lidar and the sonic anemometer, the distance traveled by the sensing volume and the distance to which the air masses are carried by the mean wind during this time will vary greatly, since the velocity of the mean wind is substantially less than the linear velocity of movement of the sensing volume at the base of the scanning cone. We believe that in order to compare the results of estimating the dissipation rate, it is more appropriate to use the lidar data and the acoustic anemometer data, which correspond to the same distances.

k) p. 12 line 5: Is it possible to discern that the increase in kinetic energy computed over more scans (over longer time periods) is truly a better measure, and not simply due to non-stationarity of the mean wind (as discussed for the stable case at line 15) increasing the variances across the entire conical scan? Based on Fig. 6, the mean wind changes (wind speed slowly decreases, direction shifts) over the 6 hour time window mentioned, thus this may be causing the increase in measured TKE.

The variance of the average (30-minute averaging) of the wind velocity, calculated from the data in Figure 6 (a) for a height of 200 m and a time interval from 12:00 to 18:00, is approximately 10 times less than the TKE given in Table 1 (for 30 scans). Therefore, we can assume that the contribution of the nonstationarity of the mean wind to the kinetic energy estimate is negligible, in comparison with the turbulent fluctuations of the wind field. However, for another case considered in the manuscript (measurement at an altitude of 200 m from 01:00 to 07:00), the variance of the average (30-minute averaging) of the wind velocity is approximately twice the estimate of the kinetic energy obtained by using lidar data for 30 scans. This is the reason that, with an increase in the averaging interval from 10 min to 60 min, the magnitude of the kinetic energy estimate is monotonically increasing (it has no saturation, as in the first case under consideration). Apparently, for conditions of very weak turbulence on the background of nonstationarity of the mean wind, a special procedure for data filtering is required, which is not the subject of this paper.

l) p. 12 line 15: Other possible reasons include the inability of the lidar to resolve any portion of the inertial subrange (thus all derived parameters are not valid) and the low bias of dissipation (denominator for calculation of integral scale) when it is small.

We agree with this comment. Under conditions of stable thermal stratification of the atmosphere, the inertial subrange of turbulence can be much smaller than the size of the sensing volume, or even the inertial interval may be absent. It is obvious that the method of estimating the dissipation rate and the integral scale described in the manuscript is not applicable for this case. Therefore, in this manuscript there are no results of data processing, measured by the lidar in 2016 at night.

m) p. 12 line 20-22: The meaning and significance of 'The value of . . . over azimuth angles' is unclear; it should be rewritten.

Fixed.

n) p. 13 line 2: What is meant by 'close to each other'? A quantitative measure (standard deviation or range of values) is needed.

Page 14, lines 9-10: "(maximum deviation is around 20%)" has been added.

o) p. 15 line 125: Add the qualifier here that these high estimates were under stably stratified conditions.

Probably, the reviewer has in mind line 25.
Page 17, line 14: "(measurements in the daytime)" has been added.
Page 17, line 16: the sentence "Sometimes such estimates exceed 1 km in contrast to results shown in Figures 6(f), 7(d) and 8(d)." has been added.

p) End of manuscript: With the large number of variables and subscripts in this manuscript, adding a list of the symbols would be extremely helpful in reading this manuscript. I had to keep searching through the paper to find variables that were first introduced many pages earlier in the paper.

Pages 17-20: Appendix with a list of symbols has been added.

Technical corrections:
a) p. 6 line 10 (and reference list): 'Pearson' not 'Pierson'

Fixed.

b) p. 6 line 20: Should σe2 have an overbar as well?

Page 6, lines 25-26: The sentence "In Eqs. (13) and (14) it is assumed that $\sigma_e$ is independent of the azimuth angle $\theta_m$" has been added.

c) P. 11 line 15: 'continuously' is a better word than 'permanently'.

Fixed.

**Referee #2**
General comments:

This manuscript presents a methodology for deriving turbulent parameters from scanning Doppler lidar observations in the lower atmosphere. The methodology is sound and the results show that the parameters derived from Doppler lidar measurements usually agree well with reference parameters obtained from a sonic anemometer. The methodology uses a particular turbulence model which dictates how certain properties of the observed turbulence are expected to behave and so enable them to be derived.
A clear statement describing atmospheric situations when this model is applicable, and situations when it is not likely to be applicable, should be included in the conclusion. Are there methods for checking whether the turbulence model is applicable in a particular situation? For example, can you use the Doppler lidar observations to check for stationarity? In addition, what are the likely biases if the model is not strictly applicable, but provides reasonable results? An example here is the slight underestimates in turbulent energy dissipation rate provided by the Doppler lidar at low values. Is this expected because of unrealistic integral scales used, or is it an issue in accounting for radial velocity measurement uncertainty correctly?

To answer these questions, more research is needed. In this manuscript, we propose a method that is applicable for determining the parameters of wind turbulence from lidar measurements in the atmospheric layer of intensive mixing. The turbulence model, on the basis of which this method was developed, is quite applicable for such a layer. To obtain information about wind turbulence from measurements by a lidar in a stably stratified boundary layer (especially inside a low-level jet stream), it is necessary to apply another data processing procedure that is not known to us. Also it is necessary to take into account that at very strong stable temperature stratification the turbulence becomes intermittent and the inertial subrange can disappear.
Page 17, lines 23-25: The sentence “However, as shown by the lidar experiment conducted under stable temperature stratification outside the layer of intensive turbulent mixing (Smalikho and Bankh, 2017), this method is not applicable and, consequently, further investigations and development of new approaches are needed.” has been added.

The manuscript contains all of the information necessary for publication, but in its current state is difficult to read. There are a huge number of variables and subscripts introduced, which although necessary for completeness, make it difficult to follow. It would be easier to comprehend if large parts of the derivation were placed in an appendix, with terms directly related to the parameters that will be derived from observations included in the text. In addition, the instrument should be introduced first in Section 3, so that it is easy to refer to the instrument specifications when introducing the measurement strategy. Add a table presenting the relevant instrument specifications, e.g. pulse-repetition-frequency, receiver bandwidth/Nyquist velocity, range gate length, azimuthal scanning speed, lidar wavelength, telescope type, rather than referring the reader to another paper. As an aid to the reader, this table could also include the associated variable in the equations. After some minor modifications, I feel this manuscript will be suitable for publication.

Pages 18-20: Appendix with a list of symbols has been added.
Main parameters of the Stream Line lidar are given in Table 1 of our paper published last year in AMT (see page 10, lines 9-10). In our opinion, the inclusion of this table in the manuscript submitted to the same journal would be superfluous. The parameters of the lidar experiments conducted in 2014 and 2016 differ and are given in Sections 4 and 5, respectively.

Specific comments:
Page 1, line 19: The data provided by these instruments is not really ’raw’ data, but radial velocities.

The phrase “raw data measured” has been replaced by “measurements”.

Page 2, line 13: Suggest replacing ’were proposed’ by ’have been proposed’.

Fixed.

Page 2, line 24: Need to state that this is ’100 to 500 m in altitude’, as it could be assumed that the distances refer to range.

Fixed.

Page 2, line 27: Suggest starting the paragraph with ’First, we describe the equations that will be used to develop the measurement strategy and method for deriving the wind turbulence parameters:’

Page 2, lines 29, 30: “First of all, derive the equations to be used as a basis for development of the measurement strategy and the procedure of estimation of wind turbulence parameters:” has been replaced by “First, we describe the equations that will be used to develop the measurement strategy and the procedure of estimation of wind turbulence parameters:”.

Page 2, line 28: The measured ’raw’ radial velocities are not strictly instantaneous, as they are obtained by averaging a large number of samples internally.

Here we do not consider the radial velocity measured by a lidar.

Page 4, line 4: Suggest replacing ’some or other’ with ’an appropriate’.

Fixed.

Page 4, lines 8-9: It would be clearer for the reader if these expressions were placed on separate lines.

Fixed.

Page 3, line 15; page4, lines 20-24; and Figure 1: It should be made clear, especially in the Figure caption, that the azimuth angle refers to the azimuthal resolution (if continuous scan) or separation between 2 adjacent rays in a scan (step-stare scan).

In Section 2 we find the condition under which the azimuth structure function of the radial velocity is equivalent to the spatial transverse structure function of the wind speed. Here we do not take into account the spatial averaging of the radial velocity over the sensing volume, which takes place in lidar measurements. For a transverse structure function, it is easy to take into account the spatial averaging over the sensing volume. In our experiments we used continuous scan and, therefore, the azimuth angle resolution is equal to the angle between two adjacent rays.

Page 5, line 1: Suggest replacing ’the both’ with ’both’.

Fixed.

Page 5, line 5: What is the rationale behind choosing delta theta = 3 degrees? And what does L correspond to?

In principle, for calculation of the structure functions shown in Figure 1, we could choose any ‘delta theta’ which is less than 9 degrees (corresponding solid and dashed curves in Figure 1 almost coincide for azimuth angles less than 9 deg). In the case of ‘delta theta’ = 3 degrees and ‘L’ = 30 the maximum angle ‘delta theta’*’L’ = 90 degrees. The same ‘delta theta’ and ‘L’ were used to obtain structure functions shown in Figure 12 (in revised manuscript).

Page 5, Measurement strategy: Do you mean that you perform one conical scan with +ve azimuth rotation, then one scan with -ave azimuth rotation?

Yes.

Page 5, line 24: As defined previously, R_0 should be (delta R / 2) if the first range gate is k=0, unless you define k=0 as the first usable range gate. Then ’minimal distance’ should be defined precisely, e.g. define ’R_0 is the distance to the first usable range gate’ before the equation on line 23, and explain why the first gate should satisfy the condition stated on line 25.

Page 5, lines 24 – 25: “ $R_0$ is the distance to the first usable range gate” has been added.
“The minimal distance $R_0$ depends on the probing pulse duration. At the same time, it should satisfy the above condition $R_0 >> |< \mathbf{V} >| / (\omega_s \cos\varphi_E)$ .” has been removed. This condition must be satisfied for any ranges $R_k$ , as afore noted in Section 2 (see page 3, lines 16 – 17).

Page 5, line 26: The maximum range is effectively determined by the instrument pulse repetition frequency; the maximum usable range depends on the signal-to-noise ratio (SNR) and hence the atmosphere. Suggest rewriting this sentence, stating instead that the ’uncertainty in the radial velocity measurement depends on the SNR’.

Page 5, lines 26 – 27, page 6, lines 1 - 2: “The maximal distance … the true value of the velocity.” has been replaced by “Uncertainty in the radial velocity measurement depends on the signal-to-noise ratio (SNR). At low SNR the probability of “bad” estimate …. To avoid the application of the data filtering procedure, … not contain “bad” estimates.”

Page 6, line 9: Use correct reference (Pearson).

Fixed.

Page 6, line 11: Do you mean azimuthal dimension rather than longitudinal dimension here?

Page 6, line 12: “longitudinal” has been replaced by “transverse”.

Page 6, line 14: How do you know if Lv only occasionally exceeds the sensing volume?

Page 6, line 15: “only few times exceeds the size of the sensing volume” has been replaced by “exceeds the size of the sensing volume insignificantly”.

Page 6, lines 15-17: Other authors have shown that it is usually safer to always take account of the uncertainty in the radial velocity estimates.

Page 6, line 18: “(Frehlich et al., 2006)” has been added.

Page 6, lines 18-24: This sequence of equations requires much more explanation than is given here. ??

Text on page 6 (lines 18-24) of initial version of the manuscript has been replaced by the text on page 6 (lines 19-26) and page 7 (lines 1-3) of the revised manuscript.
Page 7, line 12: “(Banakh and Smalikho, 2013)” has been added.

Page 8, lines 12-15: Not sure that this can be justified without evidence.

Page 8, lines 18-23 and page 9, lines 1-2 (revised manuscript): The sentence “Since the instrumental error of estimation of the radial velocity … it is not necessary here to take into account the instrumental error and the effect from averaging of the radial velocity over the sensing volume.” has been replaced by “Since the instrumental error of estimation of the radial velocity … to take into account the instrumental error and the effect from averaging of the radial velocity over the sensing volume. Indeed, as shown by Eberhard et al. (1989), in the case of a horizontally homogeneous turbulence statistics and …. Taking into account that …, Eq. (25) can also be regarded as exact.”.

Page 9, line 16, and page 11, line 15: The focus of the lidar beam was set to XX m.

Fixed.

Page 11, line 9: Suggest ’To test the method for determining the kinetic energy,..’

Fixed.

Page 11, line 12-15: Suggest ’The presence of forest fires in the Tomsk region provided lidar measurements with high signal-to-noise ratios ...’

Fixed.

Page 11, line 15: Suggest replacing ’permanently’ with ’continuously’.

Fixed.

Page 11, line 20: The ’minimum useful range’.

Fixed.

Page 12, line 3: I assume you mean ’horizontal wind speed’.

Page 13, line 11 (revised manuscript): “wind velocity” has been replaced by “horizontal wind speed”.

Page 14, line 21: This assumes that the turbulent parameters don’t change over the time required to obtain 30 scans.

Page 16, line 8 (revised manuscript): “In the case of stationary conditions” has been added.

Figure 3: Suggest replacing ’Time profiles of the turbulence’ with ’Time series of the turbulent’.

Fixed.

Figure 4: Suggest replacing ’Time profiles’ with ’Time series’.

Fixed.

Figure 6: Panel (a) should state ’Wind speed’ rather than ’Wind velocity’ for the colorbar title.

Usually in our publications in English we used “Wind velocity”.

Figure 7: Suggest replacing ’Temporal profiles’ with ’Time series’.

Fixed.

Figure 7,8: Suggest replacing ’instrumental error of estimation of the radial velocity’ with ’uncertainty in radial velocity estimate’.
Figure 9: Suggest replacing ’Spatiotemporal distributions’ with ’Time-height plots’, and ’relative error of estimation of the dissipation rate’ with ’relative error in dissipation rate’.

Fixed.